

THESIS

A COMPARISON OF THE USE OF SODIUM IODIDE AND LANTHANUM BROMIDE
SCINTILLATION CRYSTALS FOR AIRBORNE SURVEYS

Submitted by

Derek M. Bailey

Department of Environmental and Radiological Health Sciences

In partial fulfillment of the requirements

For the Degree of Master of Science

Colorado State University

Fort Collins, Colorado

Spring 2014

Master's Committee:

Advisor: Thomas Johnson

Alexander Brandl
Stephen Milton

Copyright by Derek Michael Bailey 2014

All Rights Reserved

ABSTRACT

A COMPREHENSIVE COMPARISON ANALYSIS OF THE USE OF LANTHANUM BROMIDE SCINTILLATION CRYSTALS FOR AIRBORNE SURVEYS

The Environmental Protection Agency (EPA) Aerial Spectral Environmental Collection Technology (ASPECT) program performs aerial radiological and chemical characterization of geographical regions of interest. Airborne surveys are performed to characterize environmental radionuclide content, for mineral exploration, as well as for emergency scenarios such as major releases or lost sources. Two radiological detection systems are used by the ASPECT team for gamma-ray detection and characterization: lanthanum bromide [LaBr₃(Ce)] and sodium iodide [NaI(Tl)] scintillation systems. An aerial survey of a uranium mine in the western United States was performed using both NaI(Tl) and LaBr₃(Ce) detection systems. Analyses of the survey data were performed with RadAssist software and applying International Atomic Energy Agency (IAEA) airborne gamma ray mapping guidelines. The data for the survey were corrected for cross-over, which is spectral interference from higher energy photons as a result of Compton scattering, height attenuation, cosmic ray contribution to signal, and Radon contribution to signal. Two radiation survey contours were generated from each discrete data set. Based on analysis of the uranium mine survey results, LaBr₃(Ce) produced a product comparable to that of NaI(Tl). The LaBr₃(Ce) detection system contained 1/16th the scintillating volume and had a total system weight that was 1/4th that of the NaI(Tl) system. LaBr₃(Ce) demonstrated a clear advantage over NaI(Tl) detectors in system mobility, and weight factors in airborne gamma ray spectroscopy.

TABLE OF CONTENTS

ABSTRACT	ii
INTRODUCTION, THEORY, AND BACKGROUND	1
EPA's Team ASPECT	1
Aerial Surveys Background	2
Scintillators Background	3
Sodium Iodide.....	4
Intrinsic Radiation of LaBr ₃ (Ce)	5
High Purity Germanium	8
Hybrid Systems	9
Uranium Mine Survey Background	9
Survey Parameters and Equipment	10
DATA ANALYSIS.....	15
RadAssist.....	15
Live-Time Correction.....	16
Stripping Coefficients	17
Grand Junction Calibration Pads	17
Stripping Coefficient Calculation.....	20
Cosmic Coefficients	23
Height Attenuation Coefficients and Pressure correction	24
Sensitivity Coefficients	27
Data Entry	28
RESULTS	29
Stripping Coefficients	29
Cosmic Coefficients	29
Height Attenuation Coefficients.....	30
The Uranium Mine Survey Analysis.....	33
Survey Results.....	34

DISCUSSION.....	38
CONCLUSION.....	40
WORKS CITED.....	41
APPENDIX A: GRAND JUNCTION CALIBRATION PAD SPECTRA FOR NaI(Tl)	44
APPENDIX B: GRAND JUNCTION CALIBRATION PAD SPECTRA FOR LaBr ₃ (Ce)	47
APPENDIX C: STRIPPING COEFFICIENT MATRIX CALCULATION	50
APPENDIX D: COSMIC CORRECTION GRAPHS	54
APPENDIX E: HEIGHT ATTENUATION COEFFICIENT GRAPHS	56
APPENDIX F: DECAY CHAINS DOWN TO THE RADIONUCLIDE USED TO DETECT K, U, AND T.....	58
APPENDIX G: ABOUT ASPECT	59

INTRODUCTION, THEORY, AND BACKGROUND

EPA's Team ASPECT

The Environmental Protection Agency (EPA) Airborne Spectral Environmental Collection Technology (ASPECT) program, performs aerial radiological and chemical characterization of geographical regions of interest; see Appendix G for more information about ASPECT. At the time of the data acquisition, EPA's ASPECT airborne data collection system platform consisted of an Aero Commander 680 twin engine aircraft, with an array of instrumentation on board, including chemical scanners, gamma ray spectroscopy systems, a helium-3 neutron detector, a high speed digital photography system, and a real-time satellite data uplink system. Airborne radiological surveys can be complicated by a variety of variables including the geophysics of the terrain, weather conditions, rate of radiological decay, and source geometry varying from the 2π surface, for example increased signal in narrow canyons due to signal contribution from the canyon sides [1]. ASPECT uses modern data analysis methods common for airborne surveys including stripping corrections that account for gamma-ray energy cross-over, height attenuation corrections that account for gamma-ray attenuation in the air, and cosmic ray corrections which account for extra-terrestrial radiation.

Modern analysis methods in conjunction with a host of software including RadAssist by Radiation Solutions (Mississauga, Ontario, Canada); ESRI (Redlands, CA) and Google Earth (Google, Mountain View, Ca); allow ASPECT to rapidly analyze chemical and radiological data from onboard scanners in real time. The scope of the ASPECT mission includes identification of the presence of chemicals and radionuclides as well as quantifying the concentrations.

Additionally, the mission includes rendering geospatial maps that show the extent of the contamination. The goal of this research was to perform a comparison of the two different

scintillation systems that ASPECT uses, Sodium Iodide [NaI(Tl)] and Lanthanum Bromide [LaBr₃(Ce)] to ascertain the superior detector. A comparison of the performance of the two technologies was performed utilizing an environmental survey on a uranium mine.

Aerial Surveys Background

Aerial radiological surveys were originally developed for geoscience; such as mineral prospecting and geochemical mapping, as they can characterize large areas quickly in remote locations with difficult terrain [2]. In recent years, applications for airborne gamma-ray spectroscopy have been expanding into emergency situations, such as rapid response scenarios, locating lost sources, accidental releases, and national security. The EPA's ASPECT team utilizes two types of scintillation detectors: sodium iodide and lanthanum bromide. Modern gamma-ray spectroscopy utilizes advanced signal processing methods. Modern analysis algorithms have paved the way for new and innovative ways to utilize the data collected with scintillation detectors, such as ASPECT's geospatial mapping techniques.

Airborne gamma-ray spectroscopy surveys typically follow guidelines set forth by the IAEA, specifically IAEA-TECDOC-1363 (2003), and IAEA Technical Reports Series No. 323 (1991). Surveys are usually flown in a grid pattern of parallel lines; the spacing between the lines can vary from 50 m to 400 m and is typically a compromise between the spatial resolution (See Figure 1) of data needed and the cost of the survey [3]. Surveys can be flown with either fixed-wing aircraft or helicopters, from 40 m to 100 m height above ground level. Fixed wing aircraft typically fly at an airspeed of 50-60 m/s (97-117 knots), and helicopters typically fly surveys at a rate of 25-30 m/s (49-58 knots) [2]. Each platform has its advantages, while helicopters are able to get lower to the ground and are maneuverable in tight spaces, fixed wing aircraft can fly at greater speeds and cover large areas quickly [3].

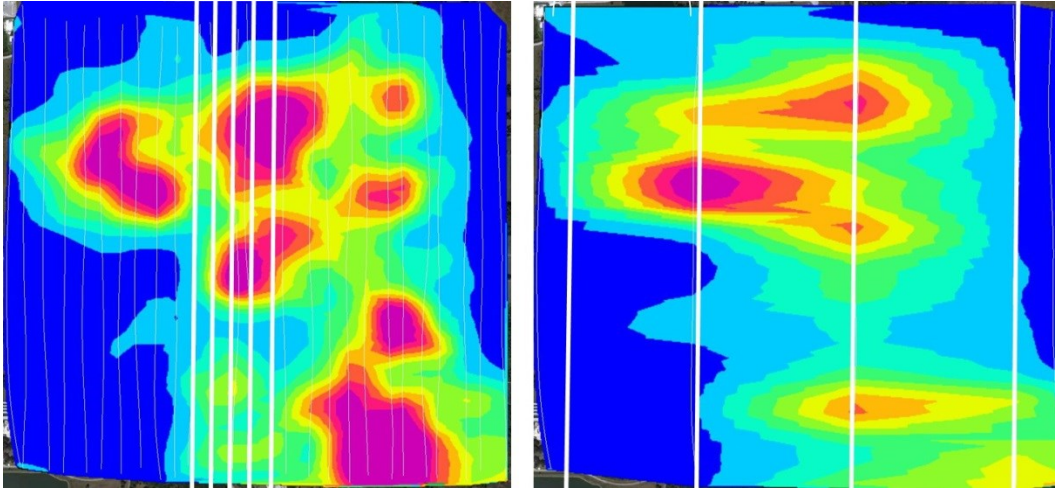


Figure 1: A comparison between line spacing and resolution. The geospatial map on the left was generated with a line spacing of 91.5 m (300 ft.), while the map on the right was generated using a line spacing of 731.5 m (2400 ft.). The maps were from an identical location [28].

Scintillators Background

Scintillators convert the energy of radiation into light photons via excitation and ionization that occurs inside the scintillating medium. Photons of visible light created inside the scintillating medium are directed into a photomultiplier tube where the light undergoes photon-electron conversion and electron multiplication creating a current pulse that is proportional to the initial ionizing event. The ability to sort radiation interactions by energy is what makes scintillators useful in the identification of a radioactive source. Scintillation technology has been used to detect the presence of radiation since the early 1900's with the development of the spintharoscope, however scintillators did not attain a high level of reliability until the invention of the photomultiplier (PM) tube in the 1940's [4]. By the mid-1950's sodium iodide scintillation detectors coupled with PM tubes were introduced and in widespread use. Today, over 60 years later, the principal technology of scintillation detectors remains very similar [5].

Sodium Iodide

Sodium iodide scintillating mediums have been in widespread use since the 1950's [5]. NaI(Tl) detectors are used in many industries and have been posited to be the optimal detector for aerial surveys. Newer scintillating mediums have been developed, both organic and inorganic, that show considerable advantages over NaI(Tl), such as higher light output, better energy resolution, and faster timing capability. However, the availability of NaI(Tl) in large volumes at a relatively low cost is possibly responsible for its continued popularity spanning a broad array of applications today [5].

NaI(Tl) scintillators typically boast a light yield of approximately 39,000 photons/MeV and a light decay time of 250 ns, with a resolution of 6.5% at 662 keV [6]. A comprehensive comparison between properties of NaI(Tl) and LaBr₃(Ce) is presented in Table 1. NaI(Tl) crystals were a natural choice for airborne gamma-ray surveys due to their compact size and broad energy response range which covers naturally occurring radionuclides and nearly all man-made gamma-ray emitting radiation sources [7].

Lanthanum Bromide

One of the most well-known alternatives to NaI(Tl) scintillation crystals is a lanthanum halide known as lanthanum(III) bromide (LaBr₃(Ce)). LaBr₃(Ce) is lanthanum tri-bromide crystal with a cerium doping agent that is commonly called lanthanum bromide in the industry. Discovered in 2001, lanthanum bromide has superior scintillating characteristics over NaI(Tl), including higher absorption efficiency, a high light yield of up to 65,000 photons/MeV, superior energy resolution as low as 2.8% at 662 keV, and a light photon decay time as low as 16 ns (Table 1) [6]. In addition, the denser LaBr₃(Ce) crystal has a higher gamma-ray absorption efficiency than NaI(Tl) per unit thickness [8].

The primary limitations of lanthanum bromide include the higher production cost, and the intrinsic radiation inside of the crystal which is discussed in the next section. Internal stress due to anisotropic thermal expansion, which is a consequence of the hexagonal structure of the crystal, in addition to $\text{LaBr}_3(\text{Ce})$ being more hygroscopic than $\text{NaI}(\text{Tl})$, has driven the need for specialized manufacturing processes and results in a more expensive product [5]. The thermal expansion properties of a $\text{LaBr}_3(\text{Ce})$ crystal cause stress build up inside the crystal during the cooling process after growth, therefore the crystals are very prone to cracking, with a likelihood that increases with crystal size. Once the crystal has cooled, however, the crystal becomes mechanically stable [6]. Modern manufacturing practices have yielded the successful growth of lanthanum bromide crystals of up to a 105×105 mm (4×4 in) cylinder, and packaged crystals available to industry are up to a 76×76 mm (3×3 in) cylindrical crystal [6]. Cost is always a consideration in any detection system comparison, but was not considered due to specific application differences.

Table 1: Comparison of key scintillating properties between lanthanum $\text{LaBr}_3(\text{Ce})$, $\text{NaI}(\text{Tl})$, [6].

	$\text{LaBr}_3(\text{Ce})$	$\text{NaI}(\text{Tl})$
Resolution (%):		
• Th-232 (2614 keV)	1.5	3.6
• Ba-137m (662 keV)	2.8	6.5
• Co-57 (122 keV)	6	8
Light Decay Time (ns)	16	250
Light Yield (photons/keV)	65	39
Density (g/cc)	5.1	3.7
Peak Emission Wavelength (nm)	380	415

Intrinsic Radiation of $\text{LaBr}_3(\text{Ce})$

Every lanthanum bromide crystal possesses a low abundance of the isotopes ^{138}La and ^{227}Ac that results in an intrinsic background of approximately $0.4 \text{ counts/cm}^3 \cdot \text{s}$ [9]. ^{227}Ac is a product of

the ^{235}U decay chain and co-exists in natural deposits of lanthanum ore. Because lanthanum and actinium are chemical analogues, separating the two is a difficult process. The most prominent signal that results from the intrinsic radiation is due to ^{138}La , which has an atomic percent abundance of 0.0902% [10]. ^{138}La decays to ^{138}Ba via electron capture (66.4%) resulting in the emission of a 1436 keV gamma-ray in coincidence with X-rays in the 35 keV region [9]. ^{138}La also decays to a metastable state of ^{138}Ce (33.6%) via beta emission with a 255 keV endpoint energy, metastable ^{138}Ce undergoes isomeric transition emitting a 789 keV gamma ray [9].

The low energy signals in the spectra represent the ^{138}La beta decay; the signal from approximately 250 keV to 750 keV is a Compton continuum from the 1436 keV and 789 keV gamma rays (See Figure 2). The apparent signal just below 1500 keV is a result of the 1436 keV gamma and the approximately 37 keV x-ray sum peak of 1473 keV. The x-ray emission by ^{138}Ba is a result of electrons dropping from higher orbitals and filling the vacant K electron shell following K-electron capture [9]. The lower energy peak partially visible on the left side of the signal around 1441 keV is a result of the 1436 keV gamma-ray emission of ^{138}La in coincidence with the 5 keV X-ray emitted by ^{138}Ba filling a vacant L-electron shell following L-electron capture [9]. According to Knoll (2010), the alpha decays associated with the ^{227}Ac decay chain are responsible for the signals from 1750-3600 keV [5]. Saint-Gobain Crystals division, Valley Forge, PA manufactured the $\text{LaBr}_3(\text{Ce})$ crystals that ASPECT uses and reported the background count rates below in Table 2 [9].

One of the potential benefits of intrinsic radiation is that the 1473 keV sum peak can potentially be used for calibration and gain-stabilization of the system without the need of a calibration source. However in low count rate scenarios, intrinsic radiation can be a hindrance. Counting environmental samples containing low activities of the primordial radionuclide ^{40}K , which

decays via electron capture to ^{40}Ar emitting a 1460 keV gamma-ray, can be prone to inaccuracy with $\text{LaBr}_3(\text{Ce})$ crystals. The energy signature of ^{40}K (1460 keV) will be masked by the 1473 keV and 1441 keV intrinsic peaks. $\text{LaBr}_3(\text{Ce})$ does not have sufficient energy resolution to fully distinguish counts between two gammas separated by as little as 9 keV; $\text{LaBr}_3(\text{Ce})$ has resolution at 1460 keV of approximately 2% making the FWHM approximately 29 keV [9]. The resulting signal from the presence of ^{40}K and the intrinsic radiation will be a peak that is actually the sum of counts between the 1460 keV emissions of in the sample and the intrinsic signal from ^{138}La inside the $\text{LaBr}_3(\text{Ce})$ crystal. Figure 3 illustrates the increased counts in the $\text{LaBr}_3(\text{Ce})$ compared to the $\text{NaI}(\text{Tl})$ crystal, the $\text{LaBr}_3(\text{Ce})$ spectrum has a larger peak around the K-40 energy.

Table 2: Intrinsic radiation count rates per unit volume of a $\text{LaBr}_3(\text{Ce})$ crystal [9].

Count Rate cps/cc	Region of Spectrum
0.226	Beta continuum from (0-225 keV)
0.065	Gamma + beta (790-1000 keV)
0.068	1468 keV gamma peak
0.034	Alpha peaks above 1600 keV

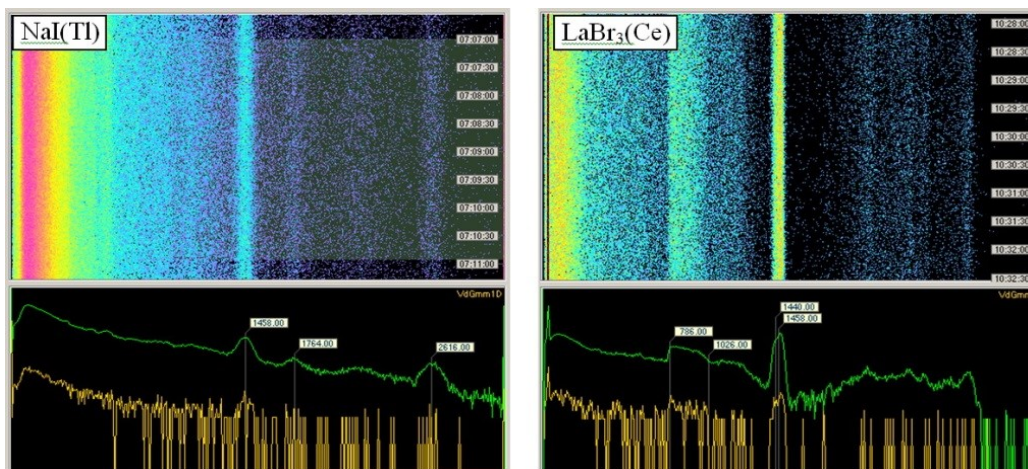


Figure 2: A Gamma-ray spectrum with corresponding water-fall illustrating the effect of the intrinsic radiation in a lanthanum bromide detector around 1460 keV. The increased count rate apparent in the potassium window of the $\text{LaBr}_3(\text{Ce})$ crystal is due to the sum of the counts of primordial ^{40}K and the counts from the intrinsic ^{138}La [28].

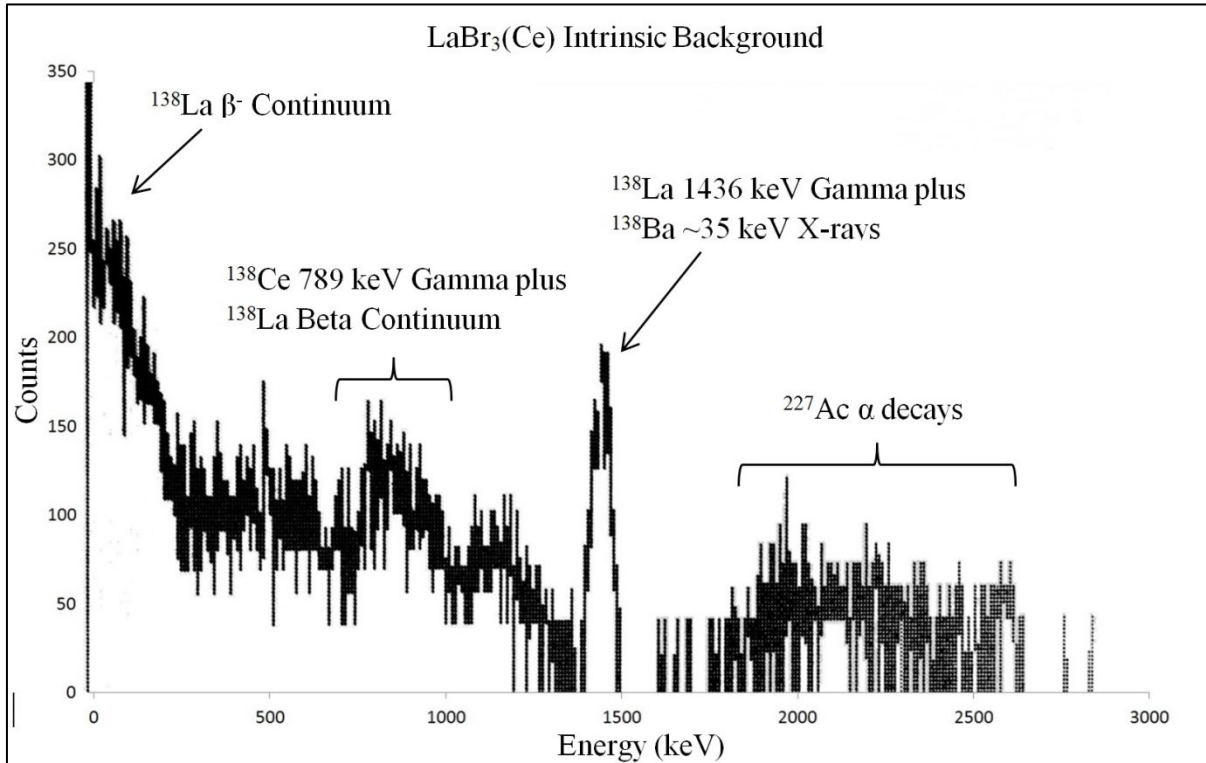


Figure 3: Intrinsic background spectrum of a 1.5'' × 1.5'' LaBr₃(Ce) Crystal. The detector was placed in a lead shield for a 13 hr count time. The low energy signal is a result of the beta decay of ¹³⁸La to ¹³⁸Ce. The continuum from 800 to 1000 keV is a continuum resulting from the 789 keV gamma emitted by ¹³⁸Ce in coincidence with the ¹³⁸La beta decay. The signal below 1500 keV is a result of the 1436 keV gamma emission of ¹³⁸La in coincidence with the ¹³⁸Ba X-rays around 35 keV. Signals above 1500 keV area due to the alpha emission of ²²⁷Ac

High Purity Germanium

High purity Germanium Detectors (HPGe) generally have superior resolution to both LaBr₃(Ce) and NaI(Tl). Historically, HPGe detectors were primarily limited to laboratory use due to the size of the apparatus and the fact that the germanium crystal must be cryogenically cooled using liquid nitrogen. However, many low power electro-mechanically cooled HPGe detectors have been developed for mobile use [11]. Scintillating crystals do not need to be continuously cooled as with HPGe detectors. Furthermore, in an emergency response scenario, or environmental survey, the primary benefit of an aerial platform is to survey large areas of land quickly in order

to identify large concentrations of radionuclides. A high level of resolution may not be necessary to accomplish the mission of emergency scenarios. As of 2013, the EPA ASPECT program was using only passively cooled radiation detection equipment.

Hybrid Systems

The EPA's ASPECT program utilizes both $\text{LaBr}_3(\text{Ce})$, and $\text{NaI}(\text{Tl})$ detectors, and research continues on combining advantages of both detectors into a hybrid system. For example, when radionuclide identification is a high priority the $\text{LaBr}_3(\text{Ce})$ portion of the system can provide approximately twice the resolution of $\text{NaI}(\text{Tl})$ and may provide more accurate (specific) radionuclide identification and better signal separation. Should the survey be over an area with very low activity and require a high level of sensitivity, the $\text{NaI}(\text{Tl})$ portion of the system is theoretically advantageous due to the superior sensitivity.

Uranium Mine Survey Background

The uranium mine surveyed was an underground mine with an onsite milling operation located in the Western United States. The specific identity and location of the uranium mine has been omitted for privacy purposes. The milling of uranium ore creates mill tailings that are the consistency of sand after the uranium ore is crushed and processed. Mill tailings are typically stored in large piles in the vicinity of the mill where the ore was originally processed. The primary radioactive component of uranium mill tailings is radium which decays to radon. The EPA has also identified other potentially harmful substances in mill tailing such as uranium, and thorium and non-radioactive constituents such as selenium and molybdenum. [12].

The EPA issued two sets of standards under the authority of the Uranium Mill Tailings Radiation Control Act of 1978 to regulate doses to the public. The standards consist of active and passive

controls enforced by the EPA, Department of Energy (DOE), and the Nuclear Regulatory Commission (NRC) that establish land restrictions for licensed mill tailing sites and minimize the contamination of water [12]. The purpose of an aerial survey is to quickly characterize a milling site to screen for elevated radiological signatures.

Survey Parameters and Equipment

Airborne radiological surveys are normally flown on a systematic grid along parallel lines (flight lines) in accordance with the International Atomic Energy Agency (IAEA) Guidelines for Radioelement Mapping (IAEA-TECDOC-1363). Two radiological detection systems were used by the ASPECT team for the uranium mine survey: LaBr₃(Ce) and NaI(Tl) scintillation systems. The uranium mine survey was performed over a 16 km × 4.8 km (10 mile × 3 mile) area and utilized flight parameters of 152 m (500 ft) line spacing at an altitude above ground level of 91.4 m (300 ft) (Figure 4).



Figure 4: 16 km × 4.8 km (10 mile × 3 mile) flight grid of the ASPECT aircraft over the Uranium mine. Flight spacing was 152 m.

During this survey, ASPECT used two discrete gamma-ray detection systems that produce independent data sets. The hardware for both systems was manufactured by Radiation Solutions Inc. (Mississauga, Ontario, Canada). The first system consisted of two RS-500 series detector packs connected to an RS-501 interface unit (Figure 5). Each RS-500 detector pack housed four $5.1\text{ cm} \times 10.2\text{ cm} \times 40.6\text{ cm}$ ($2'' \times 4'' \times 16''$) NaI(Tl) crystals for a total of 16.8 L of scintillation material, and the full system mass was approximately 109 kg (240 lbs). The second system consisted of three Radiation Solutions RSX-1 detector packs connected to an RS-701 console (Figure 5). Each RSX-1 detector pack consisted of a $7.6\text{ cm} \times 7.6\text{ cm}$ ($3'' \times 3''$) cylindrical LaBr₃(Ce) crystal for a total of 1 L of scintillating material, and the full system mass is approximately 27 kg (60 lbs) .

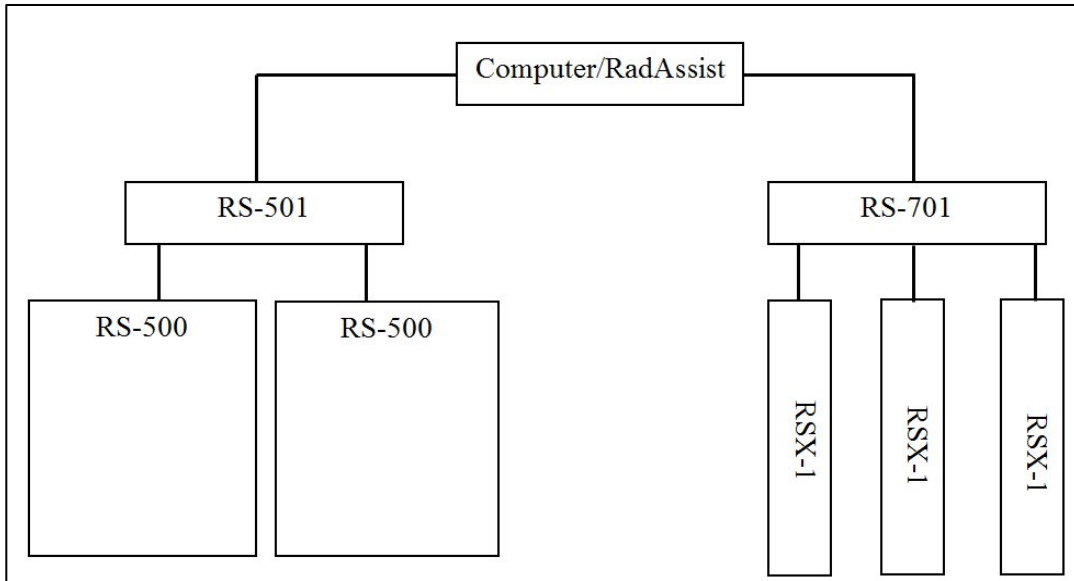


Figure 5: Line Diagram of the detector set-up. Each RSX-1 is a LaBr₃(Ce) $7.6\text{ cm} \times 7.6\text{ cm}$ crystal. Each RS-500 unit houses four $5.1\text{ cm} \times 10.2\text{ cm} \times 40.6\text{ cm}$ NaI(Tl) crystals. The RS-701 unit and the RS-500 units allow multiple detector packs to be combined into one virtual detector pack. See figure 6 for specifics.

Radiation Solutions has developed Advanced Digital Spectrometers (ADS) modules that include a built in analog to digital converter and have internal processors that drive Digital Signal

Processing (DSP) for each crystal in the array. Radiation Solutions technology allows for each crystal in the system to be used together, producing one output into the computer. The advanced DSP that Radiation Solutions utilizes allows the systems to attain throughput rates as high as 250,000 cps with < 1% pile-up contamination [13].

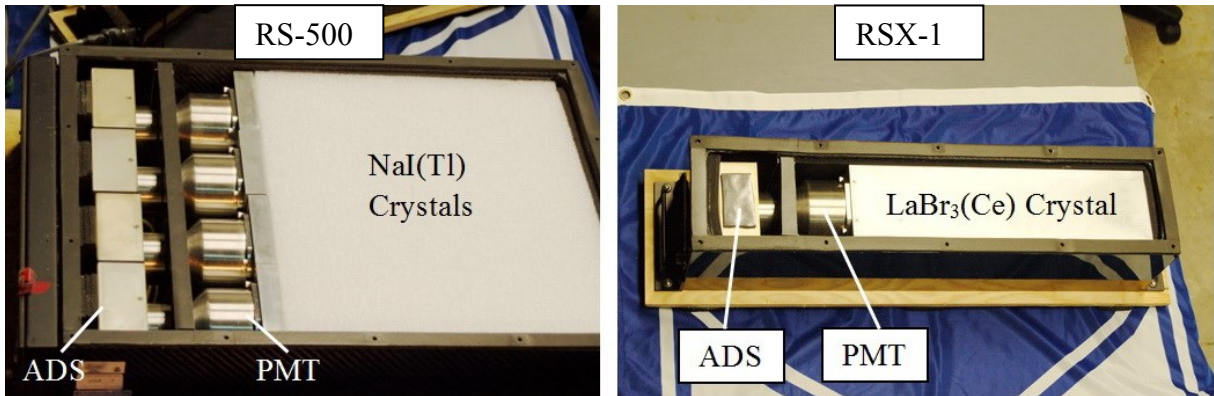


Figure 6: Internal hardware of RSX-1 and RS-500 units. Including the PMT's and ADS modules housed in a carbon fiber case.



Figure 7: RadAssist radiation detectors mounted in the tail section of the aircraft

ASPECT has conducted a series of comparisons between the two scintillating systems in order to ascertain the difference in resolution and sensitivity. Sensitivity in this paper refer to the overall sensitivity of the detector system and not the scintillating medium specifically. $\text{LaBr}_3(\text{Ce})$ has a higher cross section for absorption of photons than $\text{NaI}(\text{Tl})$ and generally has superior sensitivity [5]. However, the ASPECT $\text{NaI}(\text{Tl})$ detectors consists of 16 L of scintillation material while the $\text{LaBr}_3(\text{Ce})$ detection system consists of 1 L of scintillating material. Therefore, even though $\text{LaBr}_3(\text{Ce})$ has a higher detector sensitivity than $\text{NaI}(\text{Tl})$ at equal volumes, the ASPECT team's $\text{NaI}(\text{Tl})$ system has a higher overall system sensitivity. Due to the much larger volume of scintillating material, the $\text{NaI}(\text{Tl})$ system will register more counts than $\text{LaBr}_3(\text{Ce})$ for the same given source. Figure 8 below illustrates the superior resolution of the $\text{LaBr}_3(\text{Ce})$. The superior sensitivity of the NaI system is illustrated in Table 3.

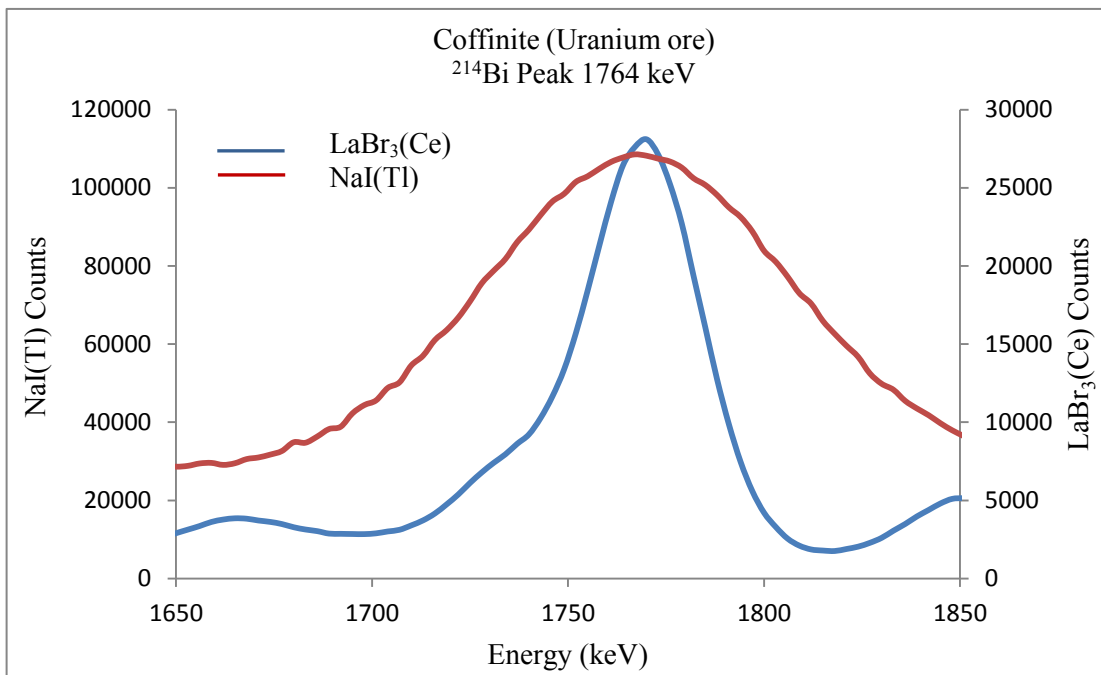


Figure 8: Resolution comparison between $\text{LaBr}_3(\text{Ce})$ and $\text{NaI}(\text{Tl})$. The counts were taken using a sample of coffinite (Uranium Ore) for approximately 100 minutes. The data were trimmed to reveal the resolution difference for the ^{214}Bi 1764 keV gamma ray.

Table 3: Total counts for each of the Grand Junction calibration pads on each system; this table reflects the raw counts for each pad over the entire energy range of the system for a collection period of approximately 100 minutes with no corrections performed on the data.

Calibration Pad	LaBr ₃ (Ce) Counts	NaI(Tl) Counts
Background Pad	1039225	7045907
Potassium Pad	1394856	12841054
Uranium pad	2351954	27982857
Thorium Pad	1736110	19016632
Mixed Pad	1977838	23125291

DATA ANALYSIS

RadAssist

ASPECT uses multiple software packages to analyze spectral data; however, for this analysis only the RadAssist software developed by Radiation Solutions Inc was used. RadAssist is a multi-faceted software package that can be used to analyze spectral data and rapidly compute concentrations, identify radionuclides, determine exposure rates, and map the extent of contamination on a contour map. RadAssist requires the following calibration parameters in order to operate effectively:

1. Counts need to be live time corrected
2. Stripping Coefficients
3. Cosmic contribution coefficients must be determined
4. Stripping corrections specific to the aspect aircraft must be computed
5. A height attenuation correction must be performed

Once all of the calibration parameters are input, RadAssist can be used to produce meaningful results from the data. The following sections will describe how to determine the appropriate calibration parameters for RadAssist, (Figure 9).

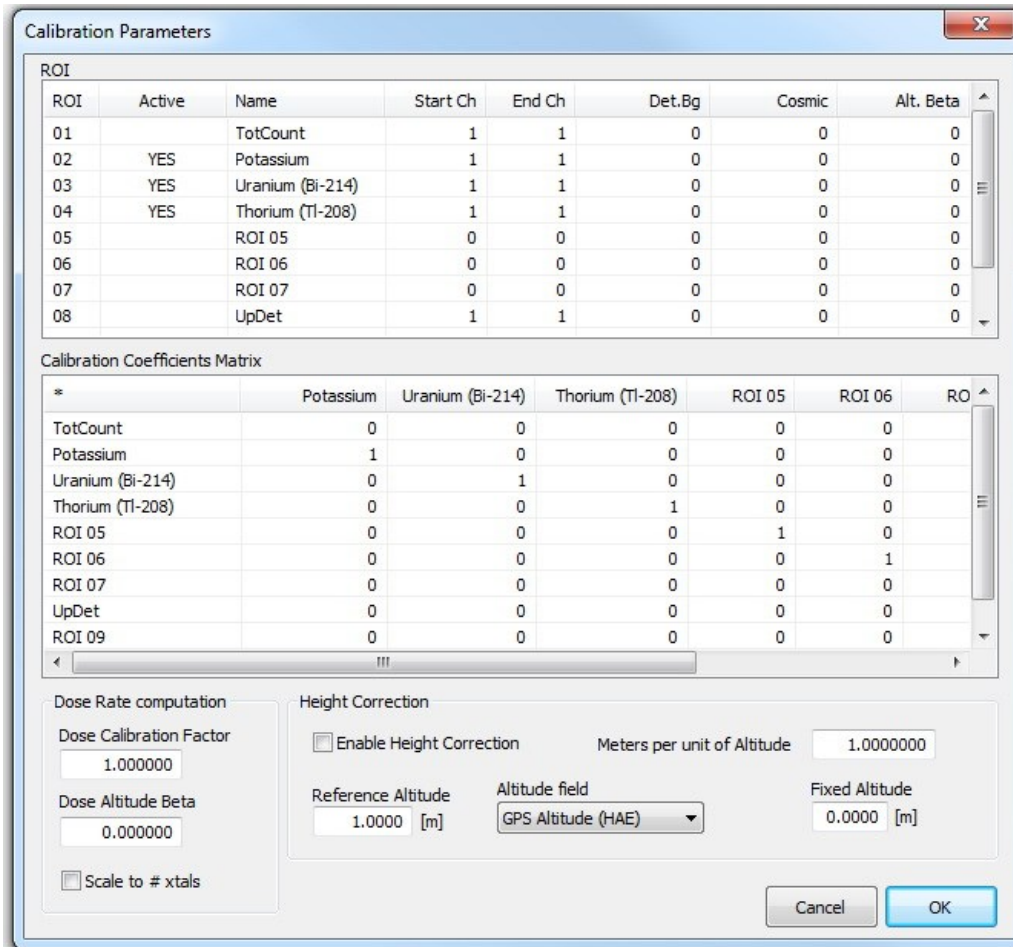


Figure 9: Default RadAssist Calibration Parameters window.

Live-Time Correction

The spectrometers that ASPECT uses require a fixed time interval to process pulses from the detector, during this time interval all other pulses are rejected. Therefore, the counting time is limited to the time taken to process all of the pulses; this is referred to as dead time. Live time is the amount of time that the system was receptive to incoming pulses [2]. All spectroscopy data were corrected for live time. ASPECT's spectroscopy system outputs two parameters, Acquired Time (μs) and Live Time (μs), Acquired Time is the amount of time that the system is active while Live Time is the amount of time the system was receptive to incoming pulses. The live time correction was made for each channel beginning with the first channel that had counts

above zero, the live time correction was used to convert the data into a count rate for each channel, see eq 1.

$$\frac{1^{\text{st}} \text{ Count above zero}}{\text{Live Time}} \cdot 10^6 \text{ s}^{-1} = \text{count rate (cps)} \quad (1)$$

Stripping Coefficients

Grand Junction Calibration pads

Stripping coefficients are developed to account for signal cross-over which is Compton interference of gamma-rays before they are detected by the system. Stripping coefficients for the ASPECT aircraft were calculated by surveying well characterized large-area calibration pads with the detectors installed in the aircraft. The calibration facility is located at Walker Airfield in Grand Junction Colorado. The calibration pads are constructed of concrete that has known concentrations of ^{40}K , ^{238}U , and ^{232}Th (K, U, T) incorporated [14]. The calibration facility was completed in 1976 for the Department Of Energy with the intended use of calibrating aircraft radiation survey instruments; the facility has also been used to calibrate vehicle based radiation detection systems [15].

The calibration facility was initially built for environmental gamma-ray spectroscopy surveys of primordial radionuclides. Careful consideration was given to the radionuclides used in the pads to achieve a gamma-ray spectrum that would be similar to a spectrum from the natural environment [15]. Airborne based spectroscopy measures potassium concentrations by utilizing the 1461 keV gamma-ray emitted by ^{40}K . Uranium concentration is measured by the 1764 keV gamma-ray emitted by its progeny ^{214}Bi , and thorium is measured by the 2615 keV gamma-ray emitted by ^{208}Tl (see Appendix F for the associated decay chains) [15]. The calibration pads

were constructed with missionary sand, a man made sand with very fine granuals; the manufacturing process of masonry sand results in a high content of angular silica from the common mineral quartz, the angular nature of manufactured sand provides strength to the complex [15]. Size 10 mesh was selected for the matrix material because its size consistency and the radioactive materials were also crushed to 10 mesh to achieve optimum homogeneity [15]. The calibration facility (illustrated in Figure 9), consists of an outdoor stretch of runway with five concrete calibration pads imbedded into the asphalt. See Table 4 below for radionuclide concentrations.

ASPECT measures uranium concentration via ^{214}Bi , which occurs far down the uranium decay chain after ^{222}Rn . The uranium daughter ^{222}Rn is a gas and may emanate both in and out of the source term material, breaking the assumption of secular equilibrium. This phenomenon is refered to as disequilibrium; as a result the uranium content can only be estimated and is reported as equivalent uranium (eU) [3]. Disequilibrium does not occur with potassium and thorium which typically maintain equalibrium in nature [3]. Although thorium is not reported as equivalent thorium, it is also suceptable to disequilibrium as ^{220}Rn progeny occurs before ^{208}Tl in the thorium decay chain. It is not possible to track radon emanation from naturally occurring sources of uranium and thorium, therefore disequilibrium introduces uncertanty into airborne gamma-ray spectroscopy.

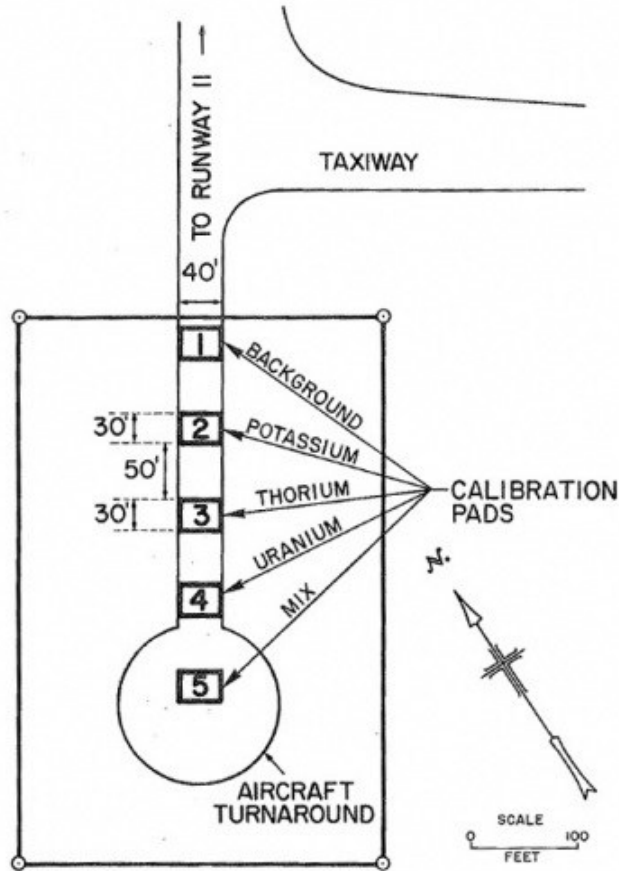


Figure 10: Each calibration pad measures 9 m × 12 m × 0.5 m (30 ft x 40 ft x 1.5 ft), pad 1 does not contain additional radionuclide content and approximates the background radioactivity, pad 2 contains a higher than background concentration of potassium, pad 3 contains a higher than background concentration of thorium, pad 4 contains a higher than background level of uranium, and pad 5 contains higher than background of all three radionuclides. Concentrations of radionuclides are given in Table 3 [14].

Table 4: Activity in Grand Junction Calibration Pads.

Pad	Activity (Bq/g)		
	K-40	Ra-226	Th-232
Background	0.4693	0.0304	0.0248
Potassium	1.6881	0.0711	0.0322
Thorium	0.6322	0.0630	0.1822
Uranium	0.6507	0.4470	0.0385
Mixed	1.2844	0.3096	0.0707

Stripping Coefficient Calculation

Gamma-rays interact with matter before creating a signal in the detector; one important phenomenon is electron/gamma-ray interactions in atoms known as the Compton Effect. If a gamma-ray interacts with an electron of an atom, the electron becomes energized and the photon continues in an attenuated state with a lower energy. The Compton Effect results in photons reaching the sensitive region of the detector with a lower energy state than when created. As a result, gamma-rays of higher energies are deceptively counted in channels of lower energies in the detector; this is referred to as cross-over. For example, a proportion of the higher energy 2615 keV ^{208}Tl gamma-rays will collide with atoms and scatter, resulting in a variety of lower energy photons (the Compton effect), and a portion of the lower energy photons will be counted in the lower energy windows of ^{214}Bi (1764 keV) or ^{40}K (1461 keV) [16]. Stripping coefficients were developed to correct for cross-over in the K, U, and Th windows of the detector [2].

A total of six stripping ratios were computed with data collected at the Grand Junction Calibration Pads. The calibration exercise was performed with the aircraft positioned on the ground over each pad for approximately 10 min. The notation used for the ratios of counts in a lower energy window to those in a higher energy window are α , β , and γ . The notation for the ratios of counts detected in a high energy window to those detected in a low energy window are a, b, and g [16].

α - (Th into U stripping ratio) = The counts detected in the U window as a ratio to those detected in the Th window from a pure Th source.

$$\alpha = \frac{S_{\text{U,Th}}}{S_{\text{Th,Th}}} \quad (2)$$

β - (Th into K stripping ratio) = The counts detected in the K window to those detected in the Th window from a pure Th source.

$$\beta = \frac{S_{K,Th}}{S_{Th,Th}} \quad (3)$$

γ - (U into K stripping ratio) = The counts detected in the K window to those detected in the U window from a pure U source.

$$\gamma = \frac{S_{K,U}}{S_{U,U}} \quad (4)$$

a - (reversed Th into U stripping ratio) = The counts detected in the Th window to those detected in the U window from a pure U source.

$$a = \frac{S_{Th,U}}{S_{U,U}} \quad (5)$$

b - (reversed Th into K stripping ratio) = The counts detected in the Th window to those detected in the K window from a pure K source.

$$b = \frac{S_{Th,K}}{S_{K,K}} \quad (6)$$

g - (reversed K into U stripping ratio) = The counts detected in the U window to those detected in the K window from a pure K source.

$$g = \frac{S_{U,K}}{S_{K,K}} \quad (7)$$

Total count rate measurements for the K, U, Th windows were taken on the calibration pads and then are linearly related to the known K, U, and Th concentrations of each pad [17].

$$n_K = s_{K,K}c_K + s_{K,U}c_U + s_{K,Th}c_{Th} + b_K \quad (8)$$

$$n_U = s_{U,K}c_K + s_{U,U}c_U + s_{U,Th}c_{Th} + b_U \quad (9)$$

$$n_{Th} = s_{Th,K}c_K + s_{Th,U}c_U + s_{Th,Th}c_{Th} + b_{Th} \quad (10)$$

Where:

n_K = K window count rate

n_U = U window count rate

n_{Th} = Th window count rate

c_K = K pad concentration

c_U = U Pad concentration

c_{Th} = The pad concentration

s_x = Window sensitivities

Each of the equations n_K , n_U , and n_{Th} , have four unknowns. The number of unknowns was reduced to three by subtracting the count rates and concentrations of the background pad from the K, U, and Th pads [16]. The unknowns were then computed in matrix form below where N is the count rate matrix, S is the sensitivity matrix, and C is the concentration matrix [16]

$$N = SC \quad (11)$$

$$\begin{bmatrix} n_{K,K} & n_{K,U} & n_{K,Th} \\ n_{U,K} & n_{U,U} & n_{U,Th} \\ n_{Th,K} & n_{Th,U} & n_{Th,Th} \end{bmatrix} = \begin{bmatrix} s_{K,K} & s_{K,U} & s_{K,Th} \\ s_{U,K} & s_{U,U} & s_{U,Th} \\ s_{Th,K} & s_{Th,U} & s_{Th,Th} \end{bmatrix} \times \begin{bmatrix} c_{K,K} & c_{K,U} & c_{K,Th} \\ c_{U,K} & c_{U,U} & c_{U,Th} \\ c_{Th,K} & c_{Th,U} & c_{Th,Th} \end{bmatrix} \quad (12)$$

Because 3×3 matrices are invertible, the sensitivity matrix can be solved with the following:

$$N = SC$$

$$S = NC^{-1}$$

The sensitivity matrix equals the inverse of the concentration matrix multiplied by the count rate matrix. With the nine sensitivity values, the stripping coefficients α , β , γ , a , b , and g were calculated. See Table 6 in the results for the calculated stripping coefficients and Appendix C for specifics associated with the matrix calculation. The stripping normalized spectra for NaI(Tl) and LaBr₃(Ce) are shown in Appendix A and B, respectively.

Cosmic Coefficients

Count rates from cosmic radiation increase exponentially in all spectral windows as height increases. The cosmic contribution of counts was accounted for and subtracted from the spectral data [16]. IAEA guidelines were used to correct for the contribution of cosmic and aircraft contributions to the radiological signature. The correction is done by using a cosmic window that records all counts above 3 MeV in the detector. No terrestrial radionuclides have gamma-ray energies above 3 MeV so all counts in the cosmic window are assumed to be non-terrestrial radiation [16].

The cosmic window count rates were then related to the counts due to cosmic radiation in the K,U, Th spectral windows by the following linear function.

$$N = a + bC \quad (13)$$

N = The count rate in the given window

a = The aircraft background count rate for a given window (represents the Detector Background in RadAssist)

b = The cosmic stripping ratio (the counts in the given window per count in the cosmic window) (represents the Cosmic factor in RadAssist)

C = the cosmic window count rate.

The values of a and b were determined experimentally by ASPECT per IAEA 323 guidelines [17]. Five flights were performed at 915 m (3,000 ft), 1525 m (5,000 ft), 2285 m (7500 ft), 3048 m (10,000 ft), and 3810 m (12,500 ft) with a 3 min measuring time at each altitude over the Gulf of Mexico. Performing the flights over the sea and at a high altitude negates the effects of primordial radionuclides and radon in all windows, allowing the cosmic contribution to be effectively isolated.

After the data are collected at each altitude, RadAssist software is capable of exporting the raw data into a “Summed Detector Spectrum”. The summed detector spectrum is in comma

delimited format so that the spectral data can be used in Excel (Microsoft, Redmond, WA) and represents the total number of counts associated with each of the 1024 channels from the multi-channel analyzer (e.g., 0 keV to greater than 3,000 keV). A scatter plot of the data was created using the cosmic counts (channel 1024) vs. each K, U, and Th region of interest for every altitude flown. The altitudes are determined from a pressure altimeter reading. Fitting a linear regression line to the cosmic vs. K, U, and Th graphs provides the necessary calibration parameters of “Detector Background” and “Cosmic” or slope factor for the RadAssist software [17].

ASPECT flew at five different altitudes over the Gulf of Mexico to collect the cosmic correction data, the calculated averages of which are 981.7 m, 1633.3 m, 2444.2 m, 3234.4 m, and 4052.0 m. The cosmic contribution to the overall gamma ray spectrum was determined for three regions of interest; each region of interest is the sum of counts between specified channels. The regions of interest include the Potassium window, which corresponds to the channels of the 1461 keV ^{40}K gamma-ray (channels 457 to 523, or 1371 keV to 1569 keV); the Uranium window which corresponds to channels of the 1764 keV ^{214}Bi gamma-ray (channels 553 to 620 or 1569 keV to 1860 keV); and the thorium window which corresponds to the 2615 keV ^{208}Tl gamma emission (channels 803 to 937 or 2409 keV to 2811 keV). Table 7 in Results summarizes the different ROI's and the counts obtained at each altitude. A complete summary of the plotted cosmic coefficient data is presented in Appendix D. The calculated cosmic coefficients are provided in Table 8.

Height Attenuation Coefficients and Pressure Correction

An airborne survey cannot be completed at a constant height; aircraft will migrate slightly from the target height during the survey. Height can affect window count rates exponentially;

therefore height attenuation coefficients for the K, U, and Th ROI's must be determined [2]. ASPECT used Lake Mohave, NV as a calibration field for the height attenuation determination. The Height Attenuation Coefficient is referred to as the Altitude Beta in RadAssist. To calculate the Altitude Beta, ASPECT flew over land and water at various altitudes in order to determine the altitude affects associated with the detector system. Land data include radiological signatures from terrestrial sources, cosmic, radon, and aircraft contributions. Water data include radiological signatures from cosmic, radon, and aircraft contributions. Water data were then subtracted from land data to determine the radiological signature from just terrestrial sources (K, U, and T). The terrestrial data were then fit to an exponential curve fitting the form of (eq 14) below [16]. The attenuation coefficient (Altitude Beta) was then determined with the regression that was fit to the data.

$$N_h = N_0 e^{-\mu h} \quad (14)$$

Where:

N_h = the background corrected and stripped count rate

N_0 = the count rate at ground level

μ = the height attenuation coefficient

h = the height above ground level, corrected to equivalent height at STP

The background corrected and stripped count rate of the Lake Mohave data requires the use of Stripping coefficients α , β , and γ . The attenuation and scatter of gamma-rays in air must be accounted for at the aircraft height. Because gamma-rays interact with matter in the air, the stripping coefficient is affected by the aircrafts height. The IAEA has developed stripping coefficient correction factors experimentally (Table 5) which are used to correct stripping ratios as a function of height by using equations 15, 16 and 17 [16].

Table 5: IAEA standardized coefficients used to determine the increase in a given stripping ratio as

Stripping Ratio	Increase Per meter
α	0.00049
β	0.00065
γ	0.00069

The height corrected stripping ratios were then used to correct the count rates in the K, U, and Th windows. The following equations were derived in IAEA TECDOC 323 to produce the corrected count rates [16].

$$\alpha_c = \alpha + 0.00049 \text{ increase/meter} \times H_e \text{ (m)} \quad (15)$$

$$\beta_c = \beta + 0.00065 \text{ increase / meter} \times H_e \text{ (m)} \quad (16)$$

$$\gamma_c = \gamma + 0.00069 \text{ increase/ meter} \times H_e \text{ (m)} \quad (17)$$

The height attenuation coefficients for K, U, and Th are developed with data that are collected at various altitudes to characterize the attenuation of gamma-rays as a function of height. The effective height was determined with the IAEA method presented below [16].

$$H_e = H \frac{273.15}{T + 273.15} \frac{P}{1013.25} \quad (18)$$

H = Observed height (m)

H_e = equivalent height at STP (m)

T = air temperature in (degrees C)

P = barometric pressure (mbar)

The barometric pressure and temperature readings were obtained from an internet site called weather underground [18] for a nearby weather station and were recorded for the day of the survey, the correction for height above ground level was then computed via equation 18 [2].

$$\text{Survey Pressure} = P e^{\frac{-(E + \frac{\text{AGL}}{2})}{(T \cdot 29.263)}} \quad (19)$$

P = Pressure (mbar)

E = Mid point elevation between the surface elevations and the aircraft AGL (m)

AGL = above ground level altitude (m)

T = Temperature in (C)

The height corrected stripping ratios were then used to correct the count rates in the K, U, and Th windows. The following equations were derived in IAEA TECDOC 323 to produce the corrected count rates [16].

$$\alpha_c = \alpha + 0.00049 \text{ increase/meter} \times H_e \text{ (m)} \quad (20)$$

$$\beta_c = \beta + 0.00065 \text{ increase / meter} \times H_e \text{ (m)} \quad (21)$$

$$\gamma_c = \gamma + 0.00069 \text{ increase/ meter} \times H_e \text{ (m)} \quad (22)$$

The resulting stripped count rates at each altitude are summarized in Table 11. The count rates corrected for altitude-specific stripping coefficients were then plotted against H_e to generate a plot, and an exponential regression fit. A full summary of the plots is presented in Appendix E. The count rates for each ROI were then plotted against the equivalent height H_e . An exponential function was fit to the data to yield the altitude beta (1/m) for each K, U, and Th window presented in Table 14 in the results section.

Sensitivity Coefficients

ASPECT uses sensitivity coefficients to convert K, U and T count rates into dose rates. As of the time of the uranium mine survey (2011) ASPECT has only developed sensitivity coefficients for the NaI(Tl) system and did not use the LaBr₃(Ce) system for dose rates. Therefore, sensitivity coefficients were omitted for this research.

Data Entry

Contours were generated using RadAssist. All of the calibration parameters discussed in the data analysis section were entered into RadAssist to generate a contour. Calibration parameters can be found in Figure 11 in the results section. NaI(Tl) survey data were downloaded from the RS-501 interface unit, LaBr₃(Ce) data were downloaded from the RS-701 console. Both data sets were then loaded into RadAssist for processing. The ASPECT aircraft records data for the entire flight; therefore data points for the aircraft turn-around maneuvers must be omitted. The survey data were modified to include only the data points that were taken over the region of the uranium mine. Both modified data sets were then analyzed in RadAssist and a contour was generated for the NaI(Tl) system and one for the LaBr₃(Ce) system (Figures 12 and 13, respectively).

RESULTS

Stripping Coefficients

The Grand Junction calibration pad data was used to calculate the stripping ratios α , β , γ , a, b, and g. The stripping coefficients are summarized in Table 6. The matrix calculation is shown in Appendix C.

Table 6: Calculated Stripping Coefficients

Count ROI	Stripping Coefficients
Th into U (α)	0.456307
Th into K (β)	0.663095
U into K (γ)	0.964914
Reversed Th into U (a)	0.03924
Reversed Th into K (b)	0.001646
Reversed K into U (g)	-0.00606

Cosmic Coefficients

The count rates for K, U, Th, and cosmic ROI's at the average altitude at which the data were collected is presented in Table 7. The start and end channels represent the K, U and Th ROI's, energies 1371 keV to 1569 keV, 1569 keV to 1860 keV, and 2409 keV to 2811 keV, respectively. The cosmic channel 1023 corresponds to energies above 3069 keV.

Table 7: Count rates in the K, U, Th ROI's at the average altitude (AGL) that the data were collected

Isotope	Start Chan	End Chan	982 ft	1,633 ft	2,444 ft	3,234 ft	4,052 ft
Potassium (cps)	457	523	13.27	13.92	17.30	23.25	30.74
Uranium (cps)	553	620	4.61	6.08	9.33	13.02	19.52
Thorium (cps)	803	937	5.32	6.61	10.59	15.69	21.77
Cosmic (cps)	1023	1023	123.08	151.88	221.04	313.88	447.87

The count rates for each K, U, and Th ROI were plotted against the cosmic ROI, and a trend line was fit to the data. The slope of the trend line is used as the cosmic coefficient (Cosmic)

calibration parameter in RadAssist. The cosmic coefficient is used to account for the cosmic contribution to the raw data. A linear function was fit to the data; the y-intercept of the function represents the aircraft/detector contributions to the raw data and is used in the detector background (Det.Bg) calibration parameter in RadAssist. See appendix D for a complete summary of the cosmic coefficient graphs.

Table 8: Cosmic coefficients

ROI	Cosmic Coefficient (CPS/meter)	Aircraft Background (CPS/ROI)	R ²
Potassium	0.0554	5.7721	0.995
Uranium	0.0453	0.8757	0.9988
Thorium	0.0514	0.9269	0.9976

Height Attenuation Coefficients

The geographic region of the survey had a calculated average elevation of 2150 m above sea level, a targeted survey altitude of 91.4 m (300 ft AGL) and line spacings of 152 m (500 ft). The survey was performed in August of 2011, and on the day of the survey the temperature was 80 F (26.7 C) and a survey pressure of 1015 kpa (771.9045 mbar). Weather information was obtained from a nearby airport via the Weather Underground website [18]. The environmental parameters on the day of the survey are summarized in Table 9.

Table 9: Uranium mine survey environmental parameters.

Elevation (m)	2150
Survey Altitude (m)	91.4
Temperature (C)	26.7
Pressure (mbar)	771.9
Calculated effective height (m)	105.8

The equivalent height was calculated by averaging the STP-corrected radar altimeter readings for the data collected at each reference altitude, 30.5 m (100 ft), 45.7 m (150 ft), 76.2 m (250 ft), 152 m (500 ft), 229 (750 ft), and 305 m (1000 ft). The average altimeter readings were used in conjunction with the temperature and pressure on the day of the survey to calculate the equivalent height (H_e) summarized in Table 10. The standard deviation of the average height (H) was used to confirm that the radar altimeter was functioning correctly and that the data selection process distinguishing land and water counts was performed properly.

Table 10: The equivalent height values calculated at each survey altitude over land and water.

	Target Height (m)	Average Observed Height (H) (m)	H Standard Deviation (m)	H_e (m)
Land	30.5	32.91	3.9	30.11
Water	30.5	29.54	2.07	27.03
Land	45.7	46.61	2.57	42.64
Water	45.7	45.07	2.87	41.24
Land	76.2	75.03	5.96	68.65
Water	76.2	72.8	4.86	66.61
Land	152	146.05	7.32	133.63
Water	152	153.42	2.5	140.38
Land	229	227.13	5.28	207.81
Water	229	224.88	2.25	205.76
Land	305	301.61	15.12	275.96
Water	305	298.12	4.18	272.77

The equivalent height values were then used in equations 15, 16, and 17 to compute corrected stripping ratios α_c , β_c , and γ_c at each altitude presented in Table 11.

Table 11: Height corrected stripping ratio at each equivalent height.

Target Height (m)	H_e (m)	α_c	β_c	γ_c
30.5	30.11	0.471056	0.682374	0.985479
30.5	27.03	0.469546	0.680371	0.983352
45.7	42.64	0.477195	0.690518	0.994124
45.7	41.24	0.476506	0.689604	0.993154
76.2	68.65	0.489939	0.707423	1.01207
75.2	66.61	0.48894	0.706098	1.010663
152	133.63	0.52178	0.749661	1.056906
152	140.38	0.525084	0.754044	1.061559
229	207.81	0.558129	0.797879	1.108092
229	205.76	0.557123	0.796544	1.106675
305	275.96	0.59152	0.842174	1.155112
305	272.77	0.589959	0.840103	1.152914

The count rates were analyzed to find the number of counts in the K, U, and Th ROI's, channels 457 to 523 (1371 keV to 1569 keV); channels 553 to 620 (1569 keV to 1860 keV), and channels 803 to 937 (2409 keV to 2811 keV), respectively. The counts collected over water (background) were then subtracted from the counts collected over land at each altitude to obtain corrected counts for each K, U, Th window, n_{Th} , n_U , and n_K , summarized in Table 12.

Table 12: Background subtracted count rates, in the K, U, Th windows.

Target Height (m)	H_e (m)	Potassium n_K	Uranium n_U	Thorium n_{Th}
30.5	30.11	345.2328	47.8182	58.5472
45.7	42.64	306.9716	42.853	53.8778
76.2	68.65	241.8604	34.6309	44.9397
152	133.63	139.8809	19.8487	27.4751
229	207.81	75.7393	12.9342	17.4625
305	275.96	41.4213	7.6311	10.9682

The background corrected counts were then corrected for the spectral interference that results from Compton scattering known as cross-over. The resulting count rates with cross-over correction (stripping correction) are summarized in Table 13.

Table 13: Count rates with stripping correction for each K, U, Th window.

Target Height (m)	H_e (m)	Potassium (cps) $n_{K,K}$	Uranium (eU) (cps) $n_{U,U}$	Thorium (cps) $n_{Th,Th}$
30.5	30.1	284	22.7	57.2
45.7	42.6	251.5	19.2	52.7
46.2	68.7	196.3	14.3	44.1
152	133.6	112.8	6.32	27
229	207.8	57.9	3.69	17.2
305	275	30.7	1.41	10.9

The count rates $n_{K,K}$, $n_{U,U}$, and $n_{Th,Th}$, were then plotted against the equivalent height H_e and an exponential function was fit to the data to yield the attenuation coefficients (Altitude Beta in RadAssist) for each K, U, Th window presented in Table 14. See Appendix E for the graphs associated with these results.

Table 14: Attenuation coefficients for K, U, and T windows.

	(Th)	(K)	(eU)
Attenuation Coefficient (1/m)	-0.00677	-0.00898	-0.01095
R^2	0.9998	0.9949	0.99989

The Uranium Mine Survey Analysis

Corrected stripping coefficients were calculated for the NaI(Tl) system based on the temperature and pressure corrected effective height on the day of the survey. The stripping coefficient corrections are presented in the table 15.

Table 15: Corrected stripping coefficients for the NaI(Tl) system.

	Original stripping Coefficients	Increase per meter	Stripping Coefficients for Survey
α	0.456307	0.00049	0.508136
β	0.663095	0.00065	0.731848
γ	0.976858	0.00069	1.037898

Survey Results

The following parameters were input into RadAssist (Figure 11):

- Potassium
 - ROI: Start channel 457, end channel 523
 - Det.bg: 5.772
 - Cosmic: 0.0554
 - Alt. Beta: 0.00898

- Uranium
 - ROI: Start channel 553, end channel 620
 - Det.Bg: 0.8757
 - Cosmic: 0.0453
 - Alt.Bg: 0.1095

- Thorium
 - ROI: Start channel 803, end channel 937
 - Det.Bg: 0.9269
 - Cosmic: 0.0514
 - Alt.Bg: 0.0677

- Stripping Coefficients
 - Potassium
 - i. $\gamma = 1.037898$
 - ii. $\beta = 0.731848$
 - Thorium
 - i. $b = 0.001646$
 - ii. $a = 0.03924$
 - Uranium
 - i. $g = -0.00606$
 - ii. $\alpha = 0.508136$

- Reference Altitude: 91.4 m

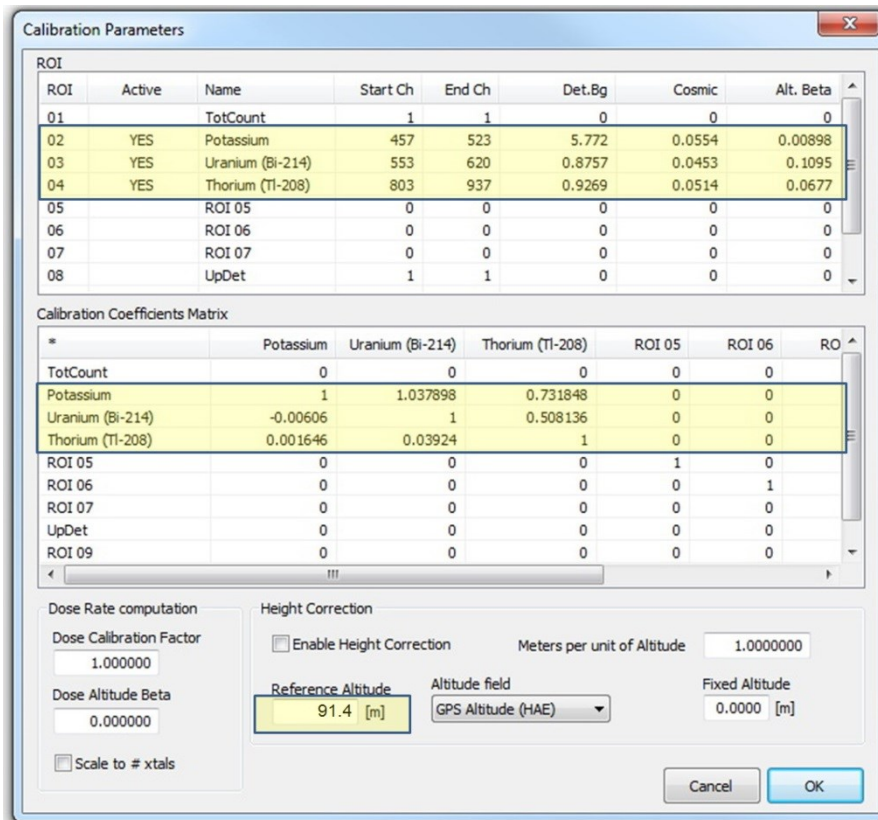


Figure 11: RadAssist Calibration parameters with the uranium mine survey parameters entered.

Two geospatial maps were produced with the discrete NaI(Tl) and LaBr₃(Ce) data sets (Figures 12 and 13). The overlay has been moved to a different geographical location to preserve the privacy of the client. The NaI(Tl) data consisted of more counts across the entire spectrum. The higher total NaI(Tl) counts were expected considering the NaI(Tl) has 16 times more scintillating volume than the LaBr₃(Ce) system. The color gradients in Figure 12 and Figure 13 were adjusted to account for the difference in sensitivity between the two systems. The color gradient for the NaI(Tl) contour corresponds to a count rate ranging from 14,000 cps to 126,000 cps. The color gradient for the LaBr₃(Ce) contour corresponds to a count rate ranging from 1000 cps to 5000 cps. The contours below represent raw count data, the LaBr₃(Ce) data were not corrected for intrinsic radiation.

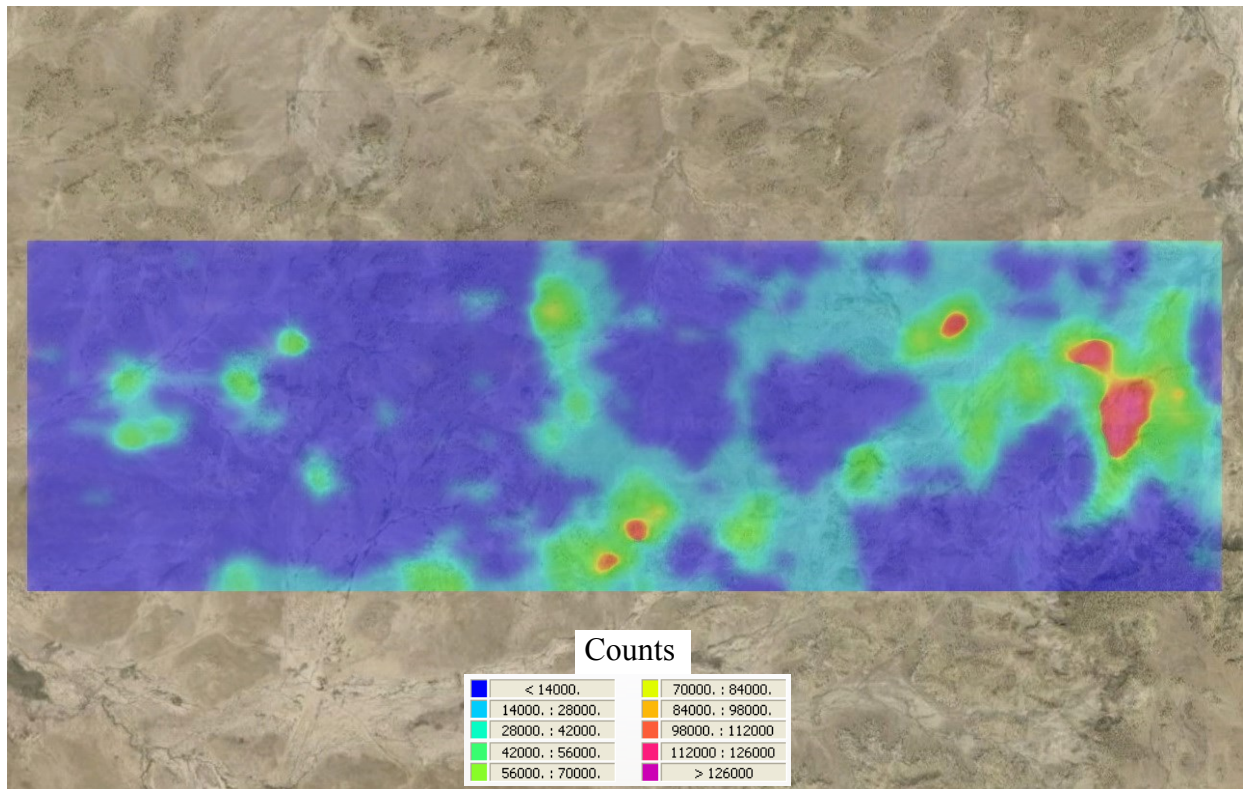


Figure 12: Geospatial contour generated from ASPECT's NaI(Tl) system, consisting of a total of 16 L scintillating volume with a total system weight of 109 kg (240 lbs)

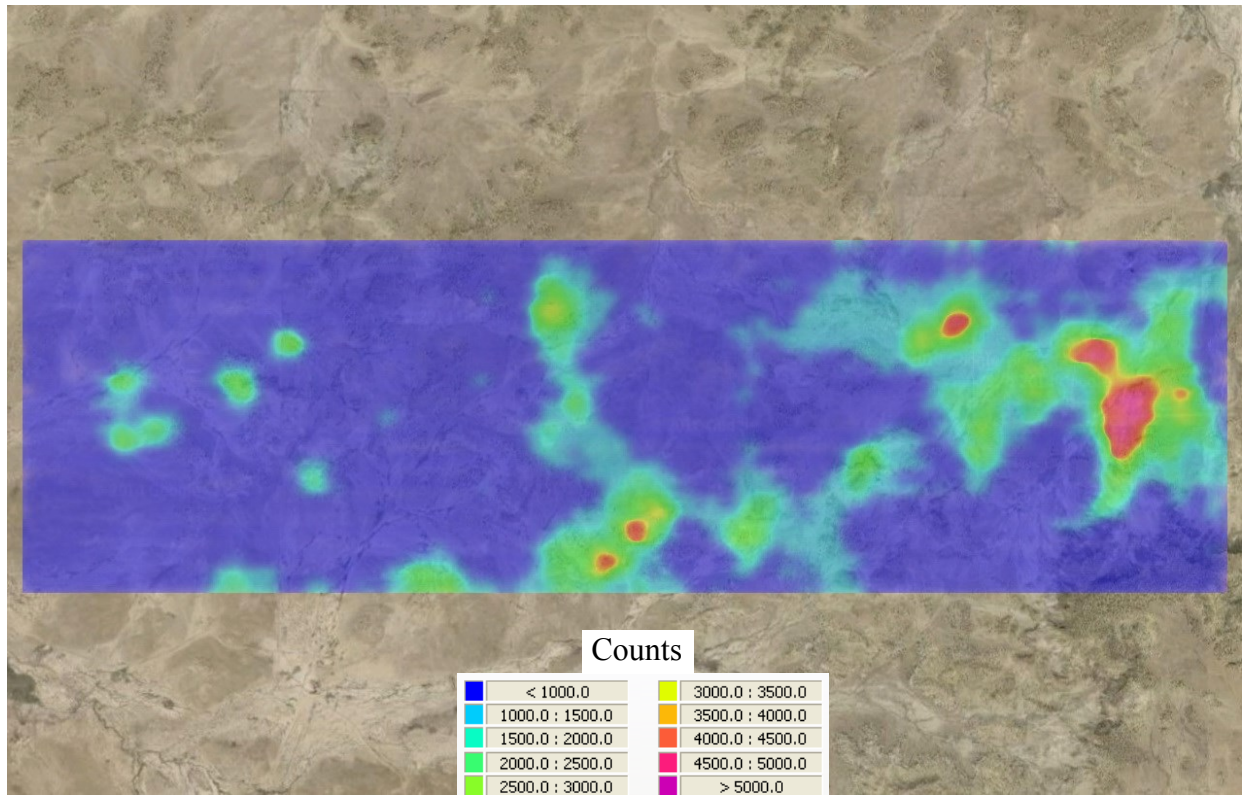


Figure 13: Geospatial contour generated from ASPECT's LaBr₃(Ce) system, consisting of a total of 1 L scintillating volume with a total system weight of 27 kg (60 lbs)

DISCUSSION

ASPECT's $\text{LaBr}_3(\text{Ce})$ system produced a commensurate product to the $\text{NaI}(\text{Tl})$ system despite the limitations of lower sensitivity and intrinsic radiation. The $\text{LaBr}_3(\text{Ce})$ can be used for airborne radiological environmental surveys without loss of resolution and with sufficient counts to distinguish artifacts from signal. A 27 kg (60 lb) $\text{LaBr}_3(\text{Ce})$ system with 1 L of scintillating volume, yielding a total count rate of 5,000 cps was used to create a nearly identical contour upon visual inspection to a 106 kg (240 lb) $\text{NaI}(\text{Tl})$ system with 16.8 L of scintillating material yielding count rates in excess of 100,000 counts. The results of this research demonstrate that low scintillating volumes are able to successfully characterize radiation from an airborne platform.

The performance of $\text{LaBr}_3(\text{Ce})$ in an environmental (low activity) survey such as this suggests that $\text{LaBr}_3(\text{Ce})$ could also be used in higher count rate scenarios where sensitivity is less important, such as emergency response, or accidental releases such as Fukushima Daiichi. In an emergency response scenario the primary role of an airborne survey is to rapidly identify where the higher concentrations of radionuclides reside (Figures 12 and 13) so that information can be communicated to ground based first responders or remediation teams. The two maps generated would very likely lead to the same ground based response for first responders or remediation teams. In a chaotic situation such as an emergency response, where system flexibility is a major advantage, the $\text{LaBr}_3(\text{Ce})$ would be superior due to its smaller size and mass. A $\text{LaBr}_3(\text{Ce})$ system of 27 kg (~60 lbs) could be easily and quickly transferred onto various platforms effectively, such as aircraft, helicopters, and vehicle based units.

Further research topics of interest would include characterizing low volume (~ 1 L) $\text{LaBr}_3(\text{Ce})$ systems in other situations that commonly utilize airborne platforms, such as high count rate situations (or simulations) such as that of a major radiological release like the Fukushima Daiichi nuclear power plant; or point source detection for finding lost sources. An ongoing topic of interest is the potential benefits of integrating lanthanum bromide and sodium iodide in a hybrid system. A hybrid system will require the development of algorithms that examine the $\text{NaI}(\text{Tl})$ and $\text{LaBr}_3(\text{Ce})$ data sets, logically selecting advantageous parameters for each crystal. Radionuclide identification and pulse discrimination would be performed with the $\text{LaBr}_3(\text{Ce})$ system, while the $\text{NaI}(\text{Tl})$ system could be used in very low count rate scenarios where high sensitivity is necessary, due to its less expensive scintillating volume to price ratio.

CONCLUSION

The role of the EPA ASPECT program is to characterize the extent and spread of chemical and radiological contamination, as well as identification of contaminant products. One of APSECT's products is contours used for environmental applications and emergency response scenarios. Two different scintillating detectors were compared in an environmental survey of a uranium mine, the industry standard NaI(Tl), and LaBr₃(Ce). The LaBr₃(Ce) system utilized in this survey had a lower scintillating volume resulting in a lower system sensitivity over the NaI(Tl) system. Other limitations of LaBr₃(Ce), such as the intrinsic radiation, called into question whether the LaBr₃(Ce) system could be successfully utilized to perform an environmental survey. Despite the limitations associated with LaBr₃(Ce), the LaBr₃(Ce) and NaI(Tl) both generated contours that would lead to the same ground based decisions for environmental surveys. The LaBr₃(Ce) system had 1/17th the scintillating volume and 1/4th total mass of the NaI(Tl) system, an important consideration for an airborne platform. LaBr₃(Ce) demonstrated a clear advantage for system mobility and mass.

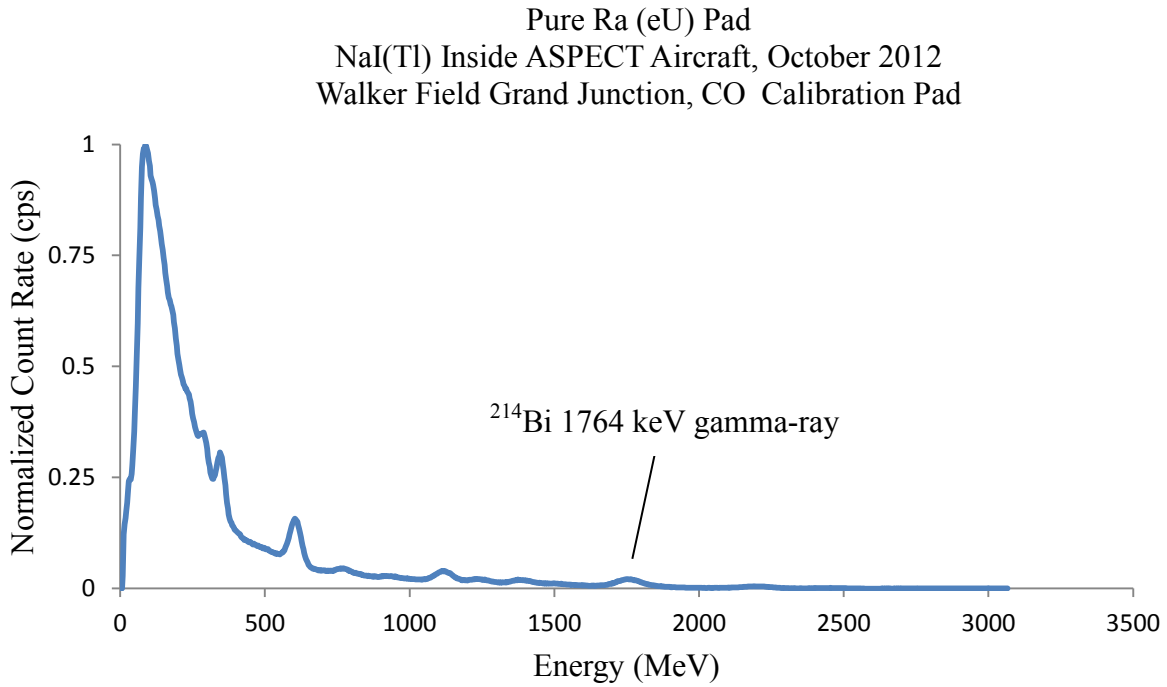
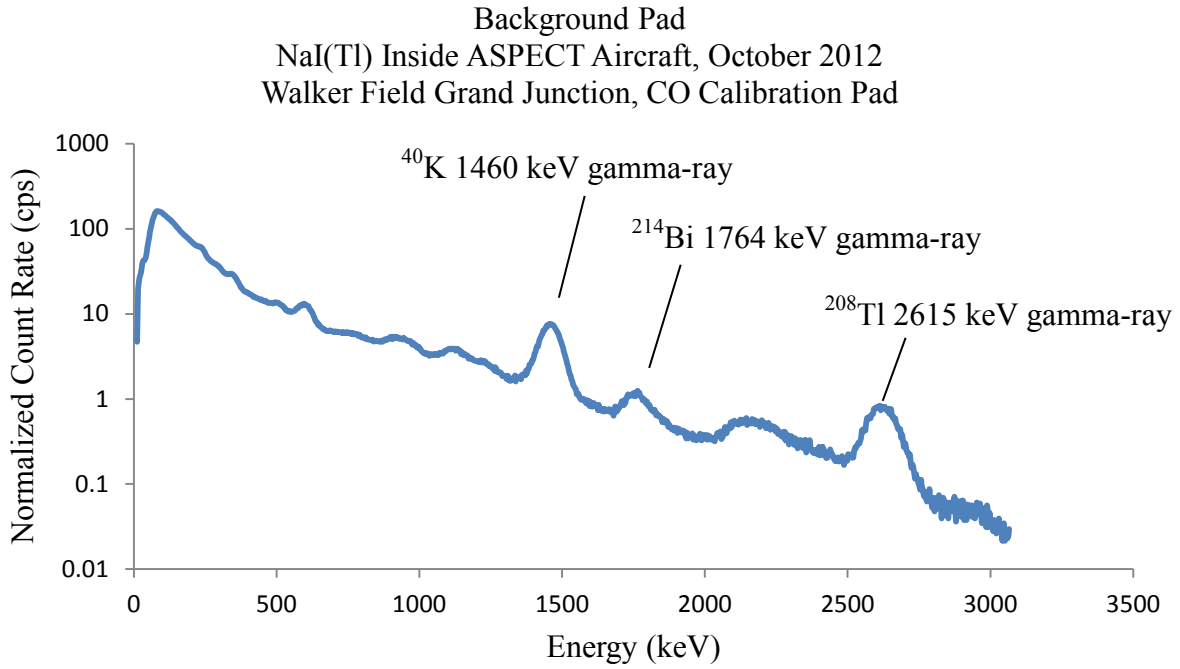
WORKS CITED

- [1] A. R. Gunn P.J, "A method for calculating equivalent layers corresponding to large aeromagnetic and radiometric grids," *Exploration Geophysics*, no. v. 28.
- [2] I. A. E. Agency, Guidelines for radioelement mapping using gamma ray spectroscopy data, Vienna, Austria: IAEA, 2003.
- [3] I. A. E. Agency, "Guidlines for radioelement mapping using gamma ray spectroscopy data," IAEA, Vienna, 2003.
- [4] W. R. Leo, Techniques for Nuclear and Particle Physics Experiments, A How-to Approach, Grunstadt Germany: Springer-Verlag, 1987.
- [5] G. F. Knoll, Radiation Detection and Measurement, Hoboken, NJ: John Wiley & Sons, Inc., 2010.
- [6] P. R. Menge, "Performance of large BrillanCe 380 (lanthanum bromide) scintillators," Saint Gobain, 2006.
- [7] A. E. Proctor, "Aerial Radiological Surveys," DOE, NV, 1997.
- [8] D. A. B. K. W. K. P. D. Mikhail S. Alekhin, "Improvement of LaBr₃:5%Ce scintillation properties by Li⁺, Na⁺, Mg⁺, Ca²⁺, Sr²⁺, and Ba²⁺ co-doping," *Journal of Applied Physics*, 2013.
- [9] S.-G. Crystals, "BrillanCe TM Scintillators Performance Summary," Saint-Gobain Crystals, Scintillation Products, 2009.
- [10] N. J. Stone, "<http://atom.kaeri.re.kr>," Nuclear Data Center, 2000. [Online]. Available: <http://atom.kaeri.re.kr/ton/nuc7.html>. [Accessed 2013].
- [11] T. T. D. U. Ronald Keyser, "Performance of Light-Weight, Battery-Operated, High Purity Germanium Detectors," ORTEC, Oak Ridge, TN.
- [12] E. P. Agency, "Uranium Mill Tailings," 8 July 2011. [Online]. Available: <http://www.epa.gov/radiation/docs/radwaste/402-k-94-001-umt.html>. [Accessed 11 Dec 2013].
- [13] R. Solutions, "RS-500 Advanced Digital Gamma-Ray Spectrometer," [Online]. Available: http://www.radiationsolutions.ca/fileadmin/pdf/RS500__Final_.pdf. [Accessed 2013].

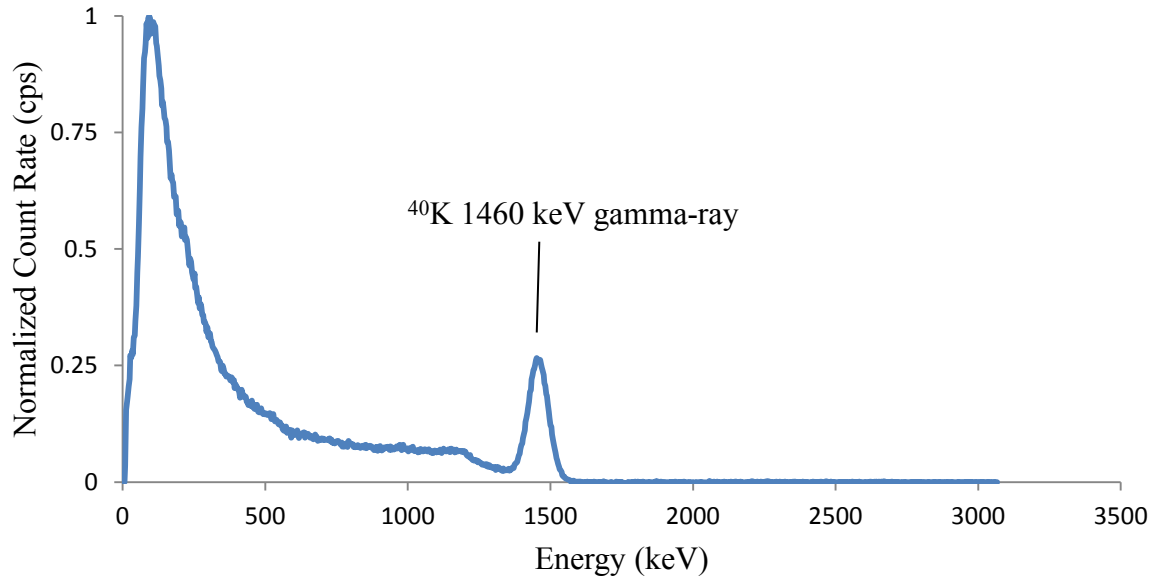
- [14] E. Novak, "Exposure-Rate Calibration Using Large-Area Calibration pads," National Technical Information Service, Springfield, 1988.
- [15] D. L. Ward, "Construction of Calibration Pads Facility Walker Field, Grand Junction, Colorado," Bendix Field Engineering Corporation, Grand Junction, 1978.
- [16] I. A. E. Agency, "Airborne Gamma Ray Spectrometer Surveying," IAEA, Vienna, 1991.
- [17] I. A. E. Agency, "Airborne Gamma Ray Spectrometer Surveying," IAEA, Vienna, 1991.
- [18] "Weather Underground," Weather Underground, Inc., 2013. [Online]. Available: <http://www.wunderground.com/>.
- [19] P. W. Frame, "Answer to Question #2345 Submitted to "Ask the Experts"," 2003. [Online]. Available: <http://archive-org.com/page/411467/2012-10-12/http://www.hps.org/publicinformation/ate/q2345.html>. [Accessed 2013].
- [20] D. A. B. K. W. K. P. D. Mikhail S. Alekhin, "Improvement of LaBr₃:5%Ce scintillation properties by Li⁺, Na⁺, Mg⁺, Ca²⁺, Sr²⁺, and Ba²⁺ co-doping," *Journal of Applied Physics*, p. 1, 2013.
- [21] E. F. Novak, "Exposure-Rate Calibration Using Large-Area Calibration Pads," Springfield: National Technical Information Service, 1988.
- [22] D. L. Ward, "Construction of Calibration Pads Facility Walker Field, Grand Junction, Colorado," Bendix Field Engineering Corporation, Grand Junction, 1978.
- [23] W. Fraczek, "Mean Sea Level, GPS, and the Geoid," 2003. [Online]. Available: <http://www.esri.com/news/arcuser/0703/geoid1of3.html>. [Accessed 10 Dec 2013].
- [24] G. Webmaster, "GEOID03," National Geodetic Survey, Apr 2011. [Online]. [Accessed 10 Dec 2013].
- [25] L. J. K. B. Rosson R, "Radiation background in a LaBr₃(Ce) gamma-ray scintillation detector.," 2011.
- [26] ORTEC, "Lanthanum Bromide Scintillation Detectors," [Online]. Available: <http://www.ortec-online.com/download/Lanthanum-Bromide-Scintillation-Detectors.pdf>. [Accessed 11 Dec 2013].
- [27] D. Roman, "COMPUTATION OF GEOID03 GEOID HEIGHT," [Online]. Available: http://www.ngs.noaa.gov/cgi-bin/GEOID_STUFF/geoid03_prompt1.prl. [Accessed 2013].

[28] J. C. II, Interviewee, [Interview]. June 2013.

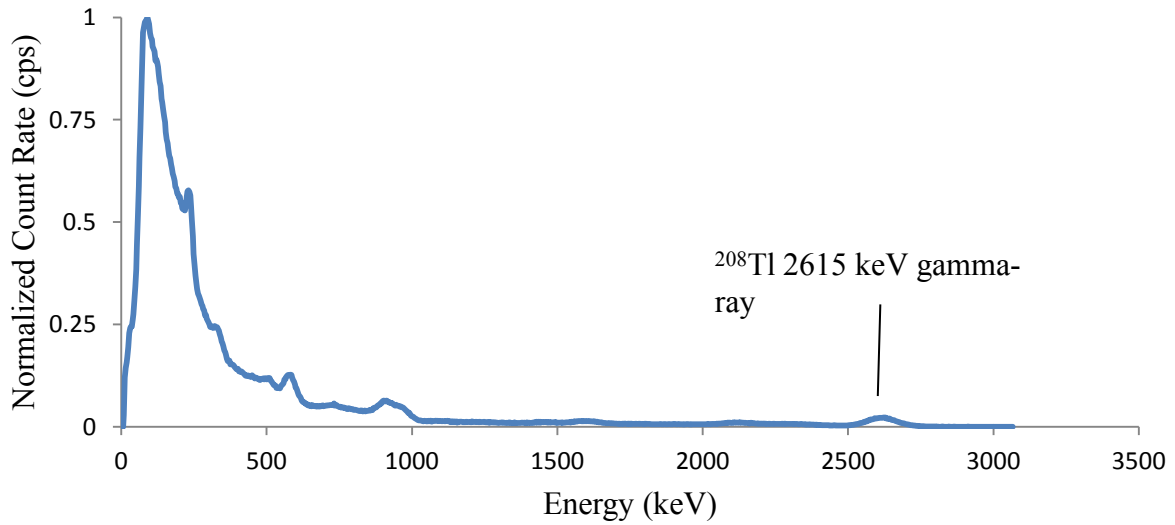
APPENDIX A: GRAND JUNCTION CALIBRATION PAD SPECTRA FOR NaI(Tl)



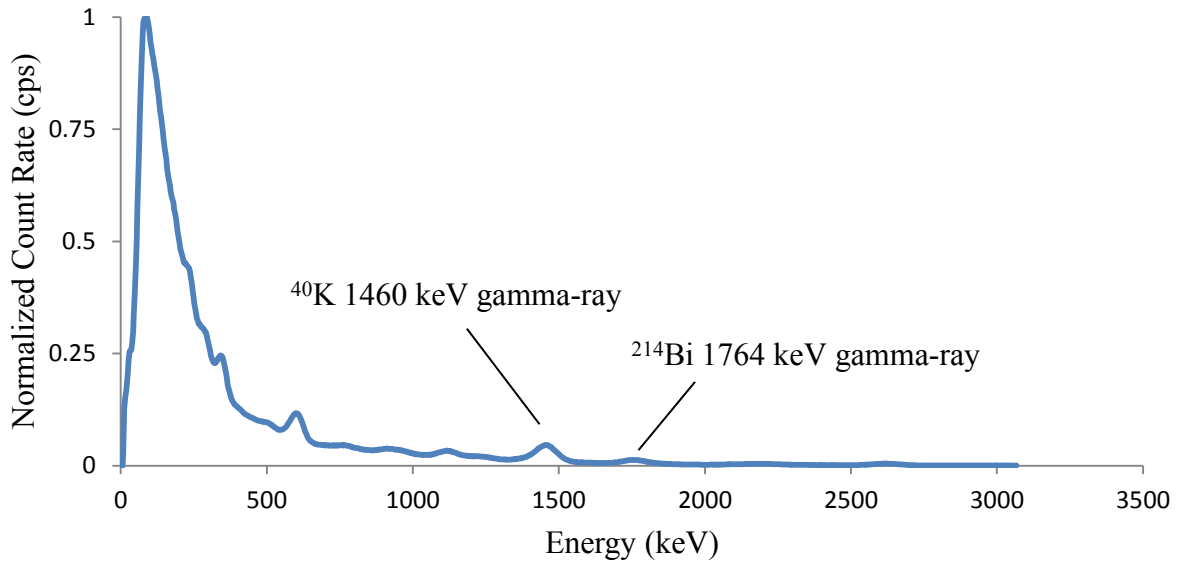
Pure K Pad
NaI(Tl) Inside ASPECT Aircraft, October 2012
Walker Field Grand Junction, CO Calibration Pad



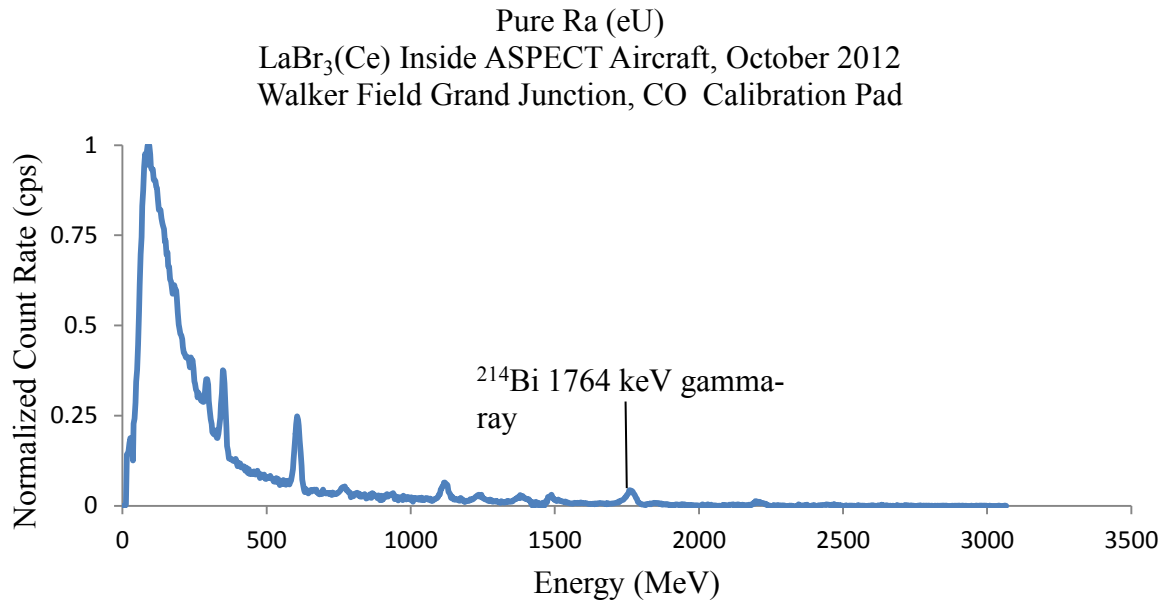
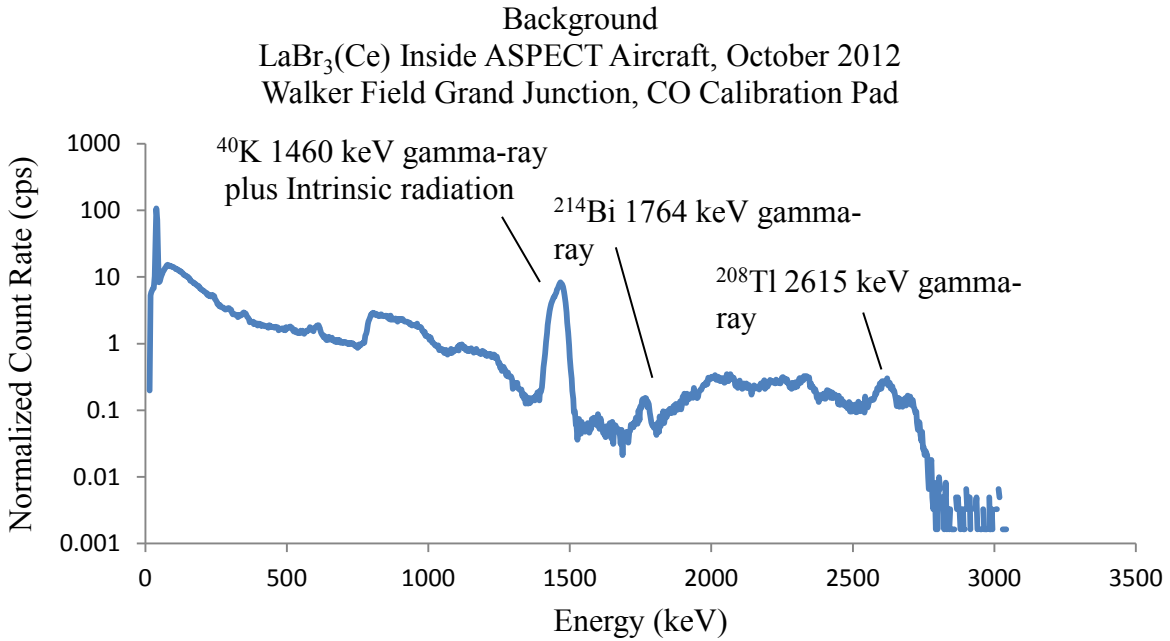
Pure Th Pad
NaI(Tl) Inside ASPECT Aircraft, October 2012
Walker Field Grand Junction, CO Calibration Pad



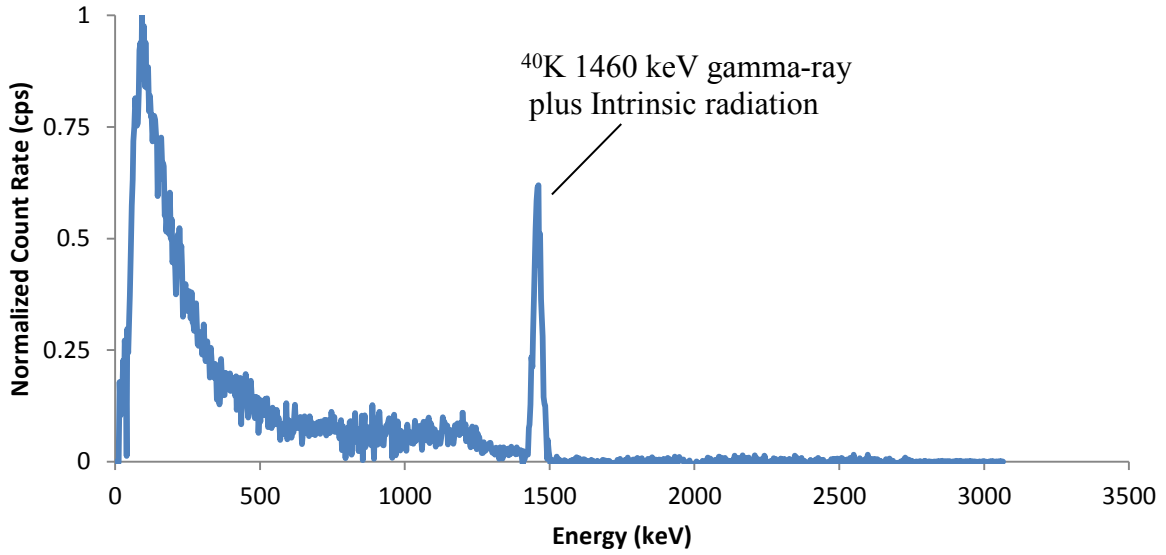
Mix Pad
NaI(Tl) Inside ASPECT Aircraft, August 2010
Walker Field Grand Junction, CO Calibration Pad



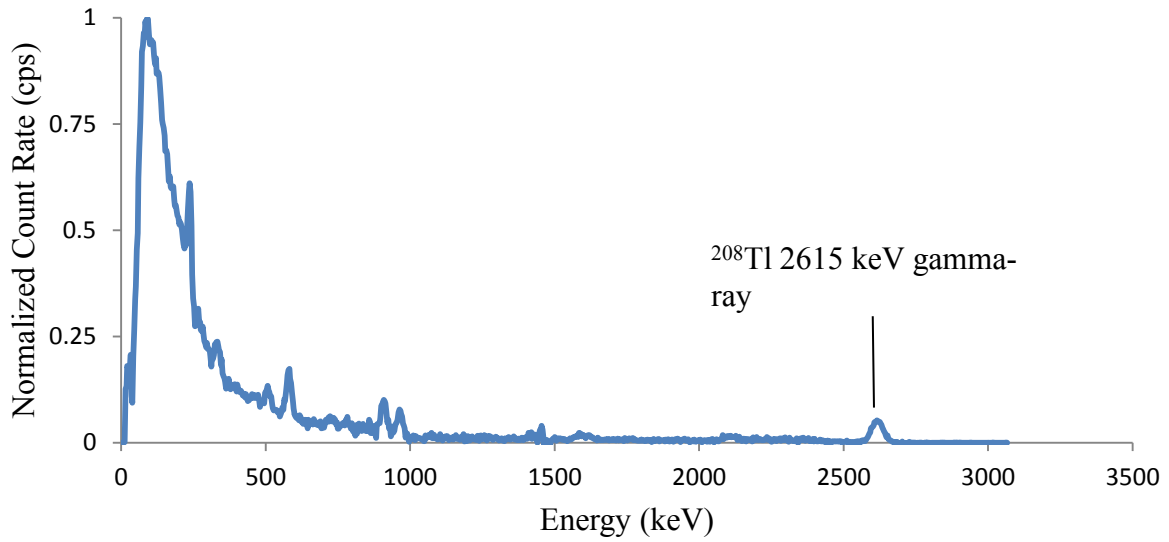
APPENDIX B: GRAND JUNCTION CALIBRATION PAD SPECTRA FOR LaBr₃(Ce)



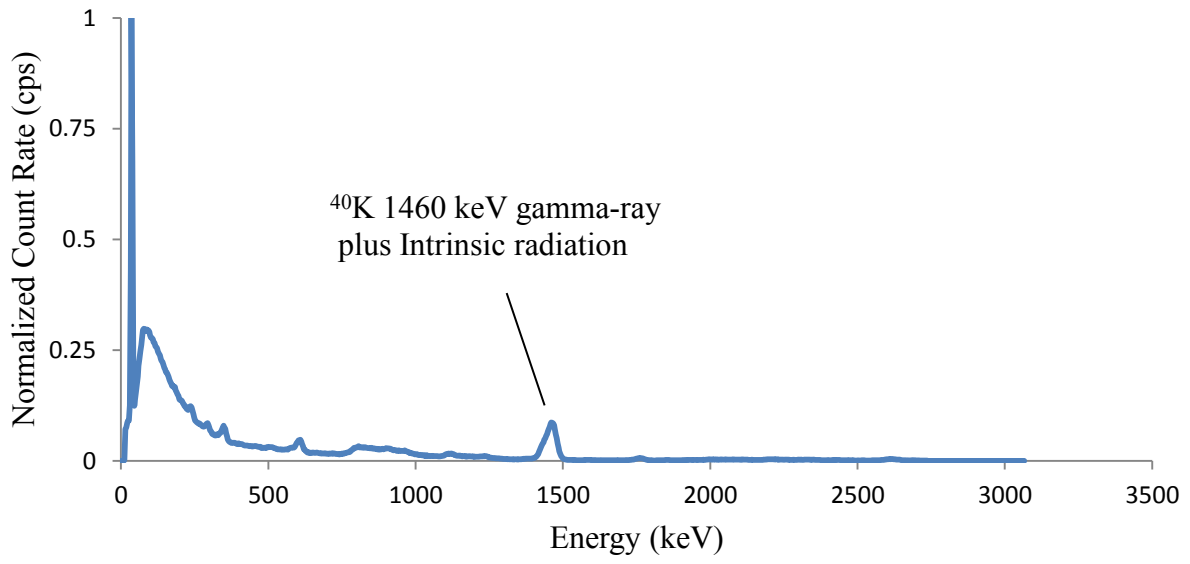
Pure K
LaBr₃(Ce) Inside ASPECT Aircraft, October 2012
Walker Field Grand Junction, CO Calibration Pad



Pure Th
LaBr₃(Ce) Inside ASPECT Aircraft, October 2012
Walker Field Grand Junction, CO Calibration Pad



Mix
LaBr₃(Ce) Inside ASPECT Aircraft, August 2010
Walker Field Grand Junction, CO Calibration Pad



APPENDIX C: STRIPPING COEFFICIENT MATRIX CALCULATION

The calibration pad concentrations were reported in pCi/g, the concentrations were converted to Bq/g with the conversion 1Bq = 27 pCi.

Pads	Concentration (pCi/g)			=	Concentration (Bq/g)		
	K-40	Ra-226	Th-232		K-40	Ra-226	Th-232
bkg -Pad	12.67	0.82	0.67		0.4693	0.0304	0.0248
K-Pad	45.58	1.92	0.87		1.6881	0.0711	0.0322
Th-Pad	17.07	1.7	4.92		0.6322	0.0630	0.1822
eU-Pad	17.57	12.07	1.04		0.6507	0.4470	0.0385
Mix ?	34.68	8.36	1.91		1.2844	0.3096	0.0707

The matrix calculation begins by filling in the concentration matrix with the calibration pad concentrations.

Concentration Matrix			=	Concentrations (Bq/g)			
				K-Pad	U-Pad	Th-Pad	
$C_{K,K}$	$C_{K,U}$	$C_{K,TH}$		K	1.6881	0.6507	0.6322
$C_{U,K}$	$C_{U,U}$	$C_{U,TH}$		eU	0.0711	0.4470	0.0630
$C_{TH,K}$	$C_{TH,U}$	$C_{TH,TH}$		Th	0.0322	0.0385	0.1822

The background pad was then subtracted from the concentrations in the concentration matrix to yield the following.

	K-Pad	U-Pad	Th-Pad
K	1.2189	0.1815	0.1630
eU	0.0407	0.4167	0.0326
Th	0.0074	0.0137	0.1574

The concentrations of uranium and thorium were converted to ppm and the potassium to percent potassium via the following conversions obtained from the Health Physics Society [19]

Uranium: 1pCi/g = 3 ppm ----> 1Bq/g = 81ppm

Thorium: 1pCi/g = 9.1ppm ----> 1Bq/g = 245.7ppm

Potassium: 1pCi/g = 1224ppm -----> 1Bq/g = 33048ppm = 3.3048 %

Finding the inverse of the concentration matrix follows the form:

$$C^{-1} = \frac{1}{|C|} [N]$$

The determinant of the concentration matrix ($|C|$) was computed

$$\begin{aligned} & [(4.0282 \cdot 33.75 \cdot 38.6750) + (0.59976 \cdot 2.6400 \cdot 1.8200) + (0.5386 \cdot 3.3000 \cdot 3.3670)] \\ & - [(0.5386 \cdot 33.7500 \cdot 1.8200) + (4.0282 \cdot 2.6400 \cdot 3.3670) + (0.59976 \cdot 3.3000 \cdot 38.6750)] \\ & |C| = 5121.35 \end{aligned}$$

The New Matrix [N]:

$$\begin{vmatrix} \begin{vmatrix} 33.7500 & 2.6400 \\ 3.3670 & 38.6750 \end{vmatrix} & \begin{vmatrix} 3.3000 & 2.6400 \\ 1.8200 & 38.6750 \end{vmatrix} & \begin{vmatrix} 3.3000 & 1.8200 \\ 33.7500 & 3.3670 \end{vmatrix} \\ \begin{vmatrix} 0.59976 & 0.5386 \\ 3.3670 & 38.6750 \end{vmatrix} & \begin{vmatrix} 4.0282 & 0.5386 \\ 1.8200 & 38.6750 \end{vmatrix} & \begin{vmatrix} 4.0282 & 0.59976 \\ 1.8200 & 3.3670 \end{vmatrix} \\ \begin{vmatrix} 0.59976 & 0.5386 \\ 33.7500 & 2.6400 \end{vmatrix} & \begin{vmatrix} 4.0282 & 0.5386 \\ 3.3000 & 2.6400 \end{vmatrix} & \begin{vmatrix} 4.0282 & 0.59976 \\ 3.3000 & 33.7500 \end{vmatrix} \end{vmatrix}$$

Determinants of each 2×2 matrix in New Matrix [N]:

$$\begin{vmatrix} 1296.39 & 122.823 & -50.314 \\ 21.3824 & 154.81 & 12.4713 \\ -16.593 & 8.85716 & 133.972 \end{vmatrix}$$

Multiply by the following alternate signs:

$$\begin{vmatrix} 1 & -1 & 1 \\ -1 & 1 & -1 \\ 1 & -1 & 1 \end{vmatrix}$$

$$\begin{vmatrix} 1296.39 & -21.382 & -16.593 \\ -122.82 & 154.81 & -8.8572 \\ -50.314 & -12.471 & 133.972 \end{vmatrix}$$

Reflect Matrix [N]:

$$\begin{vmatrix} 1296.39 & -21.382 & -16.593 \\ -122.82 & 154.81 & -8.8572 \\ -50.314 & -12.471 & 133.972 \end{vmatrix}$$

The inverse concentration matrix C^{-1}

$$C^{-1} = \frac{1}{5121.35} \cdot \begin{vmatrix} 1296.39 & -21.382 & -16.593 \\ -122.82 & 154.81 & -8.8572 \\ -50.314 & -12.471 & 133.972 \end{vmatrix} = \begin{vmatrix} 0.25314 & -0.0042 & -0.0032 \\ -0.024 & 0.03023 & -0.0017 \\ -0.0098 & -0.0024 & 0.02616 \end{vmatrix}$$

The sensitivity matrix equals the count rate matrix multiplied by the inverse concentration matrix

$$S = NC^{-1}$$

$$S = \begin{vmatrix} 473.852 & 358.183 & 214.596 \\ 29.884 & 298.303 & 114.296 \\ 11.2205 & 29.1497 & 202.612 \end{vmatrix} \cdot \begin{vmatrix} 0.25314 & -0.00418 & -0.00324 \\ -0.024 & 0.03023 & -0.00173 \\ -0.0098 & -0.00244 & 0.02616 \end{vmatrix}$$

$$= \begin{vmatrix} 109.25 & 8.32631 & 3.45901 \\ -0.71224 & 8.61411 & 2.37719 \\ 0.15069 & 0.34091 & 5.21346 \end{vmatrix} = \begin{vmatrix} S_{K,K} & S_{K,U} & S_{K,TH} \\ S_{U,K} & S_{U,U} & S_{U,TH} \\ S_{TH,K} & S_{TH,U} & S_{TH,TH} \end{vmatrix}$$

With the Sensitivity matrix, the sensitivity coefficients were calculated:

$$\alpha = \frac{S_{U,TH}}{S_{TH,TH}} = \frac{2.37719}{5.21346} = 0.45597 \quad \beta = \frac{S_{K,TH}}{S_{TH,TH}} = \frac{3.45901}{5.21346} = 0.66348$$

$$\gamma = \frac{s_{K,U}}{s_{U,U}} = \frac{8.32631}{8.61411} = 0.96659$$

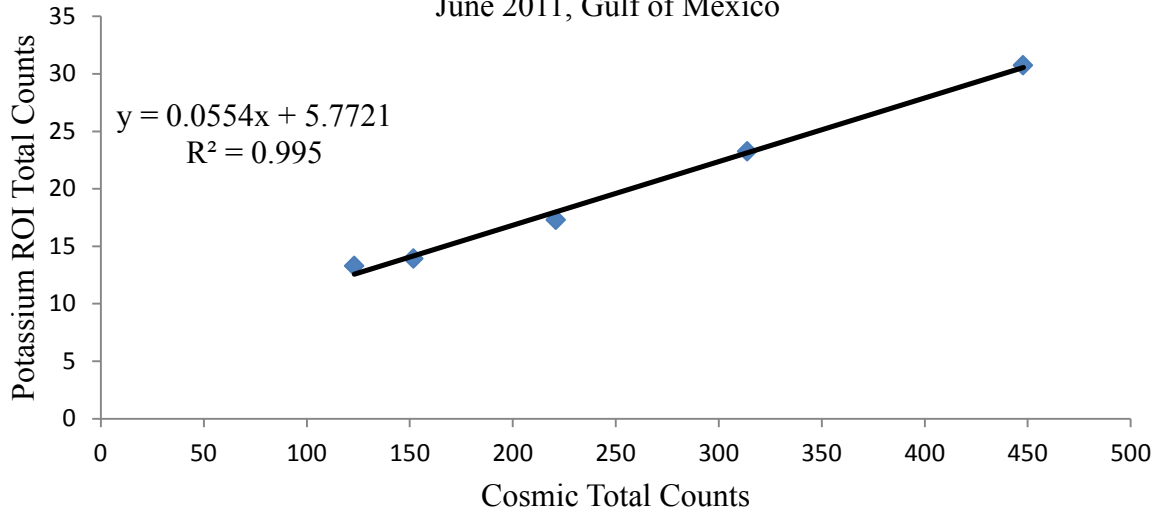
$$a = \frac{s_{Th,U}}{s_{U,U}} = \frac{0.34091}{8.61411} = 0.03958$$

$$b = \frac{s_{Th,K}}{s_{K,K}} = \frac{0.15069}{109.25} = 0.00138$$

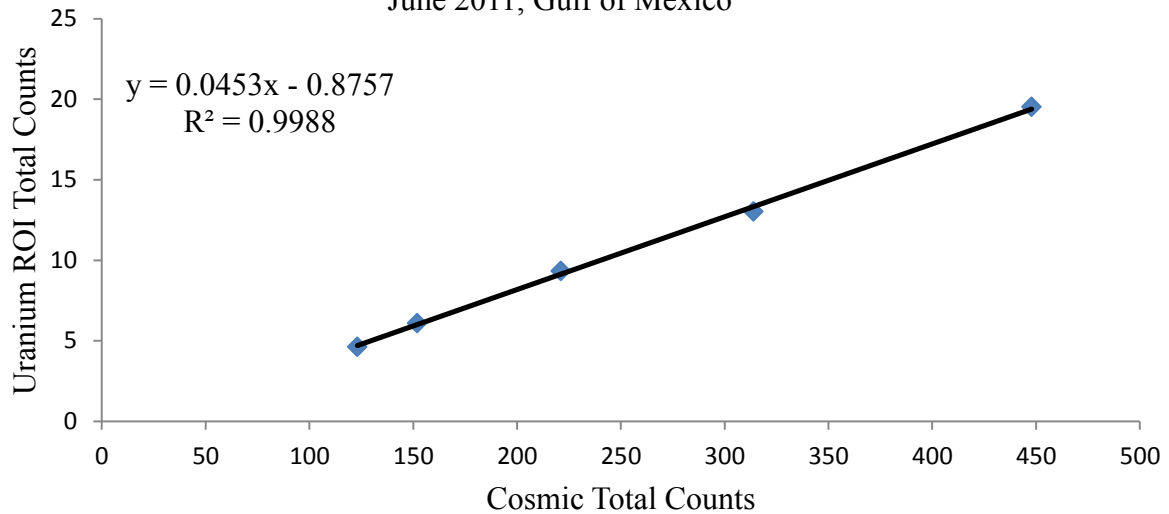
$$g = \frac{s_{U,K}}{s_{K,K}} = \frac{-0.7122}{109.25} = -0.0065$$

APPENDIX D: COSMIC CORRECTION GRAPHS

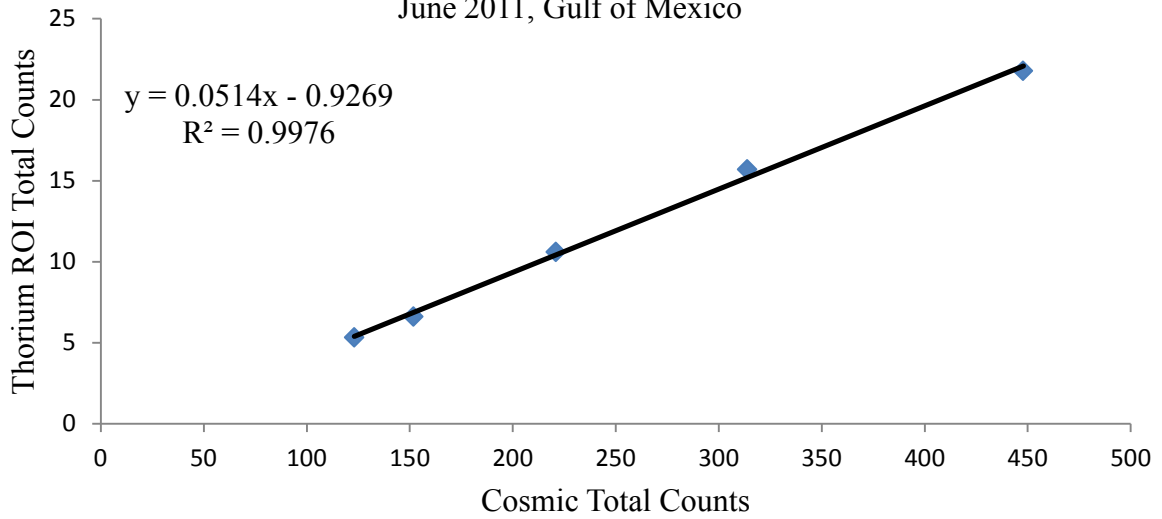
Potassium vs. Cosmic Counts
3.2K - 5.4K - 8.0K - 10.7K - 13.3K AGL Flights
Potassium ROI: Chan 457 to 523, Cosmic ROI: Chan 1023
June 2011, Gulf of Mexico



Uranium vs. Cosmic Counts
3.2K - 5.4K - 8.0K - 10.7K - 13.3K AGL Flights
Uranium ROI: 553 to 620, Cosmic ROI: Chan 1023
June 2011, Gulf of Mexico



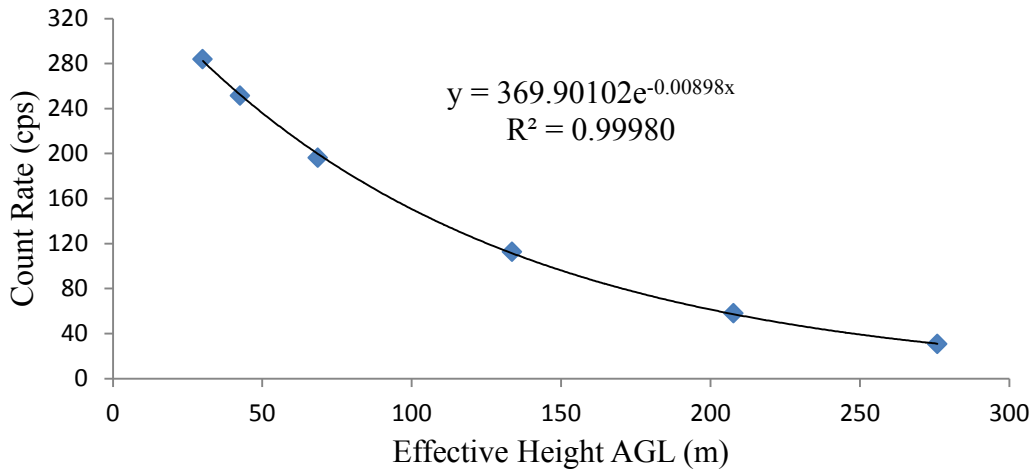
Thorium vs. Cosmic Counts
3.2K - 5.4K - 8.0K - 10.7K - 13.3K AGL Flights
Thorium ROI: Chan 803 to 937, Cosmic ROI: Chan 1023
June 2011, Gulf of Mexico



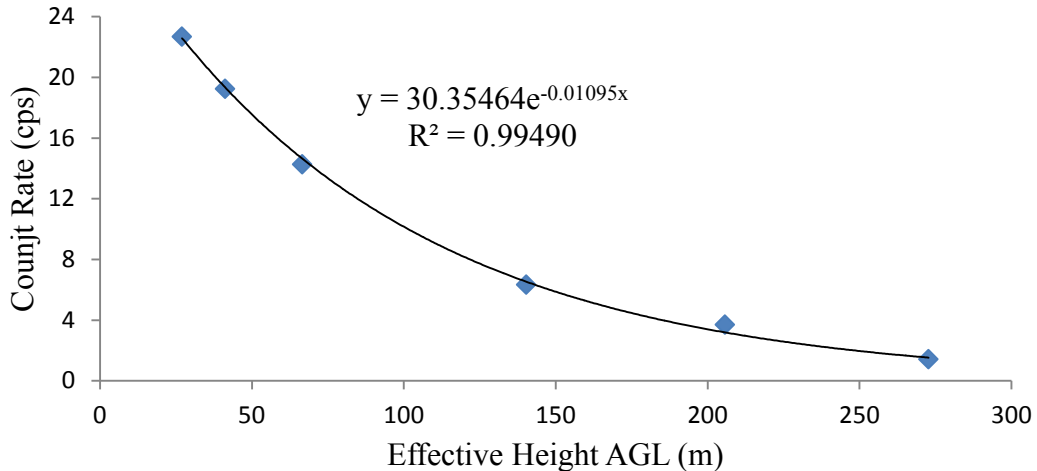
APPENDIX E: HEIGHT ATTENUATION COEFFICIENT GRAPHS

Terrestrial count rate was graphed against the Effective Height. An exponential regression was used in accordance with IAEA guidance [2] to fit the data yielding the height attenuation coefficient (Altitude Beta in RadAssist).

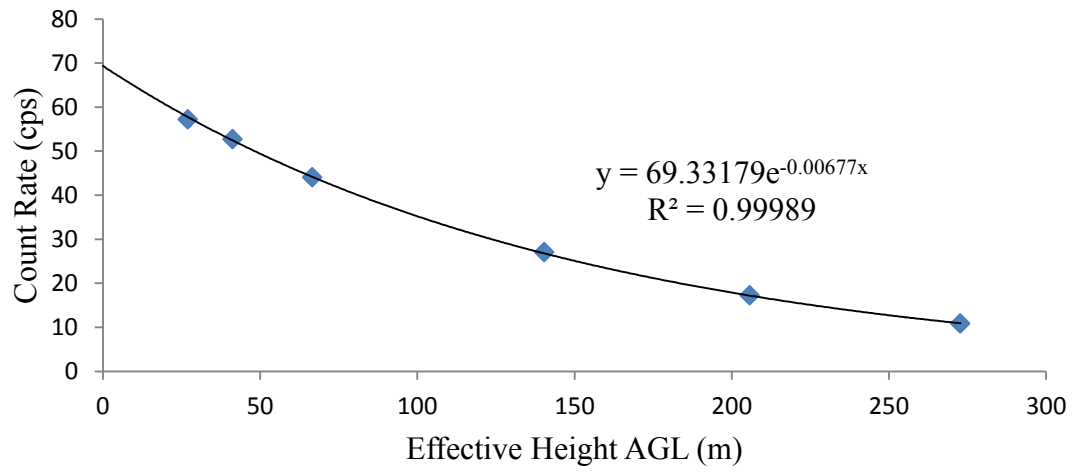
Potassium ROI
Height Attenuation Coefficient
Lake Mohave, June 28, 2011



Uranium (ROI)
Height Attenuation Coefficient
Lake Mohave, June 28, 2011

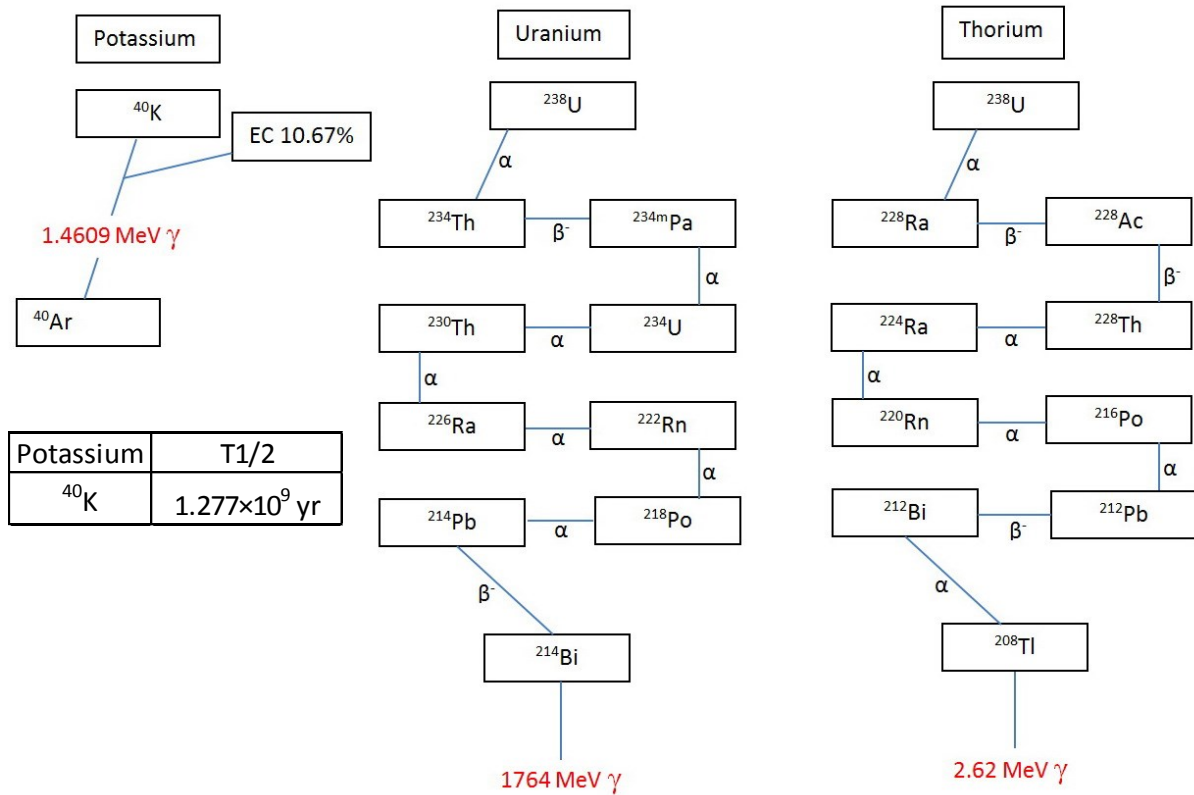


Thorium ROI
Height Attenuation Coefficient
Lake Mohave, June 28, 2011



APPENDIX F: DECAY CHAINS DOWN TO THE RADIONUCLIDE USED TO DETECT

K, U, AND T



Potassium	T1/2
^{40}K	1.277×10^9 yr

Uranium	T1/2
^{238}U	$4.468 \cdot 10^9$ yr
^{234}Th	24.10 d
$^{234\text{m}}\text{Pa}$	1.16 min
^{234}Pa	6.70 h
^{234}U	245500 yr
^{230}Th	75380 yr
^{226}Ra	1602 yr
^{222}Rn	3.8235 d
^{218}Po	3.10 min
^{214}Pb	26.8 min
^{214}Bi	19.9 min

Thorium	T1/2
^{232}Th	1.405×10^{10} yr
^{228}Ra	5.75 yr
^{228}Ac	6.25 h
^{228}Th	1.9116 yr
^{224}Ra	3.6319 d
^{220}Rn	55.6 s
^{216}Po	0.145 s
^{212}Pb	10.64 h
^{212}Bi	60.55 min
^{212}Po	299 ns
^{208}Tl	3.053 min

APPENDIX G: ABOUT ASPECT

For more information about ASPECT, the following links contain information about the program.

EPA's ASPECT Aircraft:

<http://youtu.be/cGLKoGYZGWU>

ASPECT: Flying for First Responders:

<http://youtu.be/f60r9sAozXs>

ASPECT: Behind the Science:

<http://youtu.be/uVxy-jrcnos>